

Global urban structural growth shows a profound shift from spreading out to building up

Received: 27 November 2023

Accepted: 27 June 2024

Published online: 05 August 2024

 Check for updates

Steve Frolking ¹✉, Richa Mahtta ², Tom Milliman ¹, Thomas Esch ^{3,4} & Karen C. Seto ²

We present a new study examining the dynamics of global urban building growth rates over the past three decades. By combining datasets for 1,550+ cities from several space-borne sensors—data from three scatterometers and settlement-built fraction based on Landsat-derived data—we find profound shifts in how cities expanded from the 1990s to the 2010s. Cities had both increasing building fractional cover and increasing microwave backscatter (correlating with building volume), but over the three decades, growth rates in building fraction decreased in most regions and large cities, while growth rates in backscatter increased in essentially all regions and cities. The divergence in rates of increase of these metrics indicates a shift from lateral urban expansion to more vertical urban development. This transition has happened in different decades and to different extents across the world's cities. Growth rate increases were largest in Asian cities. This shift toward vertical development has profound consequences for material and energy use, local climate and urban living.

Urban built environments grow by three processes, all of which will increase building volume: 'lateral spreading out', whereby existing nonurban lands are converted to urban areas; 'infilling', where vacant city land is built upon; and 'vertical growth', where short stature buildings are replaced by taller buildings. Three-dimensional (3D) urban structure—the patterns and spatial arrangements of land use, transportation systems and built-up infrastructure—affects greenhouse gas emissions¹, material demand² and urban climate³. Yet, despite effects of urban 3D structure on local to global environments, there is little scientific understanding or consistent empirical evidence of how the vertical dimension of global urban areas has grown and evolved over decades. This study addresses this knowledge gap.

Urban remote sensing frequently characterizes urbanization as a lateral growth process⁴ often focused on land built fraction (BF). Due to a lack of 3D information, a majority of urban growth remote sensing studies have focused on two-dimensional (2D) outward expansion⁵.

Urban BF time series data capture lateral and infill growth, but cannot directly detect building heights or even vertical growth. Although population densities were used for 3D urban representations decades ago⁶, the application of remote sensing to measure and characterize urban verticality is a relatively recent phenomenon^{7–15}. Global remote sensing studies on vertical growth have been limited to a span of about 10 years^{7,8}. Recently, methods have been developed for documenting temporal 3D change using high-resolution Synthetic Aperture Radar (SAR) data covering 3–4 years for several large metropolises^{10,11}. Several recent global high-resolution 3D studies have been limited to a single time snapshot^{12–14}. A new effort to quantify longer-term vertical trends is restricted to a single city, Beijing, combining a reference year building height data layer with backcasting from Landsat change detection¹⁵.

Active microwave backscatter is very sensitive to building physical structure through dihedral corner reflector scattering, for example, building walls and adjacent ground^{16,17}, and so to all three types of

¹Institute for the Study of Earth, Oceans, and Space, University of New Hampshire, Durham, NH, USA. ²Yale School of the Environment, Yale University, New Haven, CT, USA. ³Earth Observation Center, German Remote Sensing Data Center, German Aerospace Center (DLR), Oberpfaffenhofen, Germany.

⁴Faculty of Geomatics, Computer Science and Mathematics, Stuttgart University of Applied Sciences, Stuttgart, Germany. ✉e-mail: steve.frolking@unh.edu

urban growth. However, alone it cannot disaggregate them, in part since multiple types of growth may occur within a single backscatter grid cell (our analysis scale is 0.05° latitude/longitude or about 5 km gridding). Backscatter data have been shown to correlate spatially with building height across the span of nine US cities¹⁸, and with urban building volume at 0.05° resolution across three large regions¹⁹. Our two earlier global urban backscatter studies^{7,8} characterized urban growth during the 2000s by combining data from a single scatterometer, QSCAT, and a second independent remote sensing BF dataset, using initial state and decadal trends as metrics. These studies identified cities and regions with stronger values and trends during the 2000s in one or the other of the metrics but did not quantify changes in growth rates over time. In this study we specifically focus on the use of a multidecadal time series to address change in urban growth rates. This study advances the earlier work in several ways. We bring into the analysis global urban microwave backscatter data (henceforth PR) from two additional space-borne scatterometer datasets, the Advanced Scatterometer (ASCAT, active in the 2010s) and European Remote Sensing satellites (ERS, active in the 1990s), along with QSCAT backscatter data (active in the 2000s) used in the earlier studies. Coupling this with multidecadal World Settlement Footprint evolution (WSF-evo) BF data²⁰, we characterize changes in the rates and patterns of global 3D urban growth from the 1990s through the 2010s for 1,550+ cities. PR and BF, both space-borne measures that can detect urban growth, are fundamentally different in how they characterize urban landscapes and are completely independent measurements. Combining BF and PR data generates a more complete picture of upward and outward urban growth dynamics, here grouped into broad categories of slow growth, outward (area-dominant) growth, upward (height-dominant) growth and up-and-out (rapid 3D) growth.

Results

Mean annual BF and PR have increased over the three decades in all regions and essentially all 1,550+ cities, though rates of increase varied between regions and cities, and between decades in an individual region or city (Extended Data Fig. 1). Increases in total PR and mean BF both correlate with increases in total or new floor area at global, regional, national and metropolitan scales (Extended Data Fig. 2). In China overall, and in Beijing+ and Shanghai+, the increase in BF associated with increasing floor area has slowed recently, while the increase in PR has not (Extended Data Fig. 2e–h).

Global urban growth shifts from primarily outward to upward

We found a profound shift over time in BF and PR growth rates. Many large cities show a shift from rapid growth in BF combined with slow growth in PR (outward growth, pink shades in Fig. 1) to dominance by rapid PR and slow BF growth rates (upward growth, cyan shades in Fig. 1). Some cities have large regions of rapid growth in both BF and PR (up-and-out growth, blue shades in Fig. 1), for example, Beijing+, Ho Chi Minh City and Seoul+. There is a general pattern in megacities (population >10M) for this transition from predominantly lateral to predominantly vertical growth to occur first in the urban core area and then spread outward (Fig. 1). Only in Dhaka, with the largest population density, does this transition have a negligible pattern. In Lagos+, the northern region had very low overall BF and PR growth rates in the 1990s (gray shades). Growth in northern Lagos+ began with strong increases in BF in the 2000s, followed in the 2010s by strong increases in both BF and PR, similar to the general trend seen in Beijing+ and Ho Chi Minh City but lagging by at least a decade.

A similar shift in urban growth rate patterns occurs across most global regions (Fig. 2 and Extended Data Fig. 3). The temporal lag in this shift from rapid urban growth being predominantly outward (pink) to predominantly upward (cyan) is very apparent in an arc from East Asia through China and Southeast Asia to India (Fig. 2). Only in China are there large areas of rapid growth in both metrics (dark blue

and in many smaller cities (0.3–1M). China had 56% of the global area with rapid growth in one or both metrics (Table 1). In Indian cities, rapid growth is predominantly up-and-out or outward only in large cities (>5M) and only in the 2010s. In Europe, the transition has been negligible over the 1990s to 2010s (Extended Data Fig. 3g) while in Latin America building growth slowed over this period (Extended Data Fig. 3d). Across subregions of Africa and other Asia, the area of rapid growth has slowed substantially in South Africa from the 1990s to the 2010s, and shifted from outward to upward from the 2000s to 2010s in West Africa and Central Asia and in the most populous cities of South Asia (Supplementary Fig. 1). Across this Asian arc, median PR trends increased with increasing city population and with time, except for cities with population >5M (East Asia) or >10M (China) in 2000–2010s and in India PR trends for cities >10M less than trend for cities >5M (Extended Data Fig. 4). For these regions, median BF trends (outward expansion) generally increased with city population but decreased with time, except in East Asia (no trend with population), and in China (increased 1990s to 2000s, and no trend with population in the 2010s for cities <10M). In India the BF trend was highest for cities with a population range of 5–10M (Extended Data Fig. 4).

Globally, 80% of urban grid cells had relatively slow growth rates of both metrics in the 1990s, reducing to 74% by the 2010s (Table 1). This slower growth occurred predominantly on the periphery of large cities (for example, Fig. 1) or throughout smaller, more slowly developing cities (Fig. 2 and Extended Data Figs. 3 and 4). China was the only region with a large overall decrease in urban area with slow growth rates, dropping from 70% to 33% of total urban area (Table 1 and Fig. 2b). Of the three rapid urban growth categories (outward, up-and-out and upward), globally 80% were outward in the 1990s, dropping to 28% in the 2010s (Table 1). In aggregate, none of the increase from slow to rapid (in any category) urban growth rates happened in advanced economy countries (Table 1). Globally, from the 1990s to 2010s, outward growth area decreased 56%, while upward growth area increased ~400% and up-and-out growth area increased ~570% (Table 1). In Africa, the fraction of area with slow growth decreased in West Africa and increased substantially in Southern Africa (Table 1).

Accelerating and decelerating urban growth rates

Increasing or decreasing BF or PR growth rates from one decade to the next, that is, acceleration or deceleration in building growth rate measured by that metric, were common in several regions and most large cities (Fig. 3). China, the Middle East and East Asia had greater PR growth acceleration from the 1990s to 2000s than the 2000s to 2010s, and Africa had greater acceleration from the 2000s to 2010s (Fig. 3). Most regions had decelerating growth in BF; only China had a substantial acceleration in BF growth from the 1990s to 2000s, which then decelerated slightly from the 2000s to the 2010s but remained higher than other regions (Fig. 3). Subregionally, Central Asia had greater PR growth acceleration from the 2000s to the 2010s than South Asia, and East and West Africa had greater PR growth acceleration than North, South or Central Africa (Fig. 3). West Africa was the only subregion with accelerating BF growth from the 1990s to the 2010s (Fig. 3).

Most large cities had accelerating PR growth and decelerating BF growth, at rates larger than regional means (Fig. 3). Exceptions were Lagos+, with accelerating BF growth from the 1990s to 2000s to 2010s, and PR growth only accelerating from the 2000s to 2010s, and Beijing+, with a large acceleration in PR growth (1990s to 2000s), but a slight decline in the next decade, and offsetting BF growth acceleration (1990s to 2000s) and deceleration (2000s to 2010s).

Shifts between urban growth typologies from the 1990s to 2010s

Globally, *k*-means clustering identified seven unique clusters of urban growth across the three decades (Table 2 and Extended Data Fig. 5a–c). The characteristics of the five clusters identified in the 2000s are similar

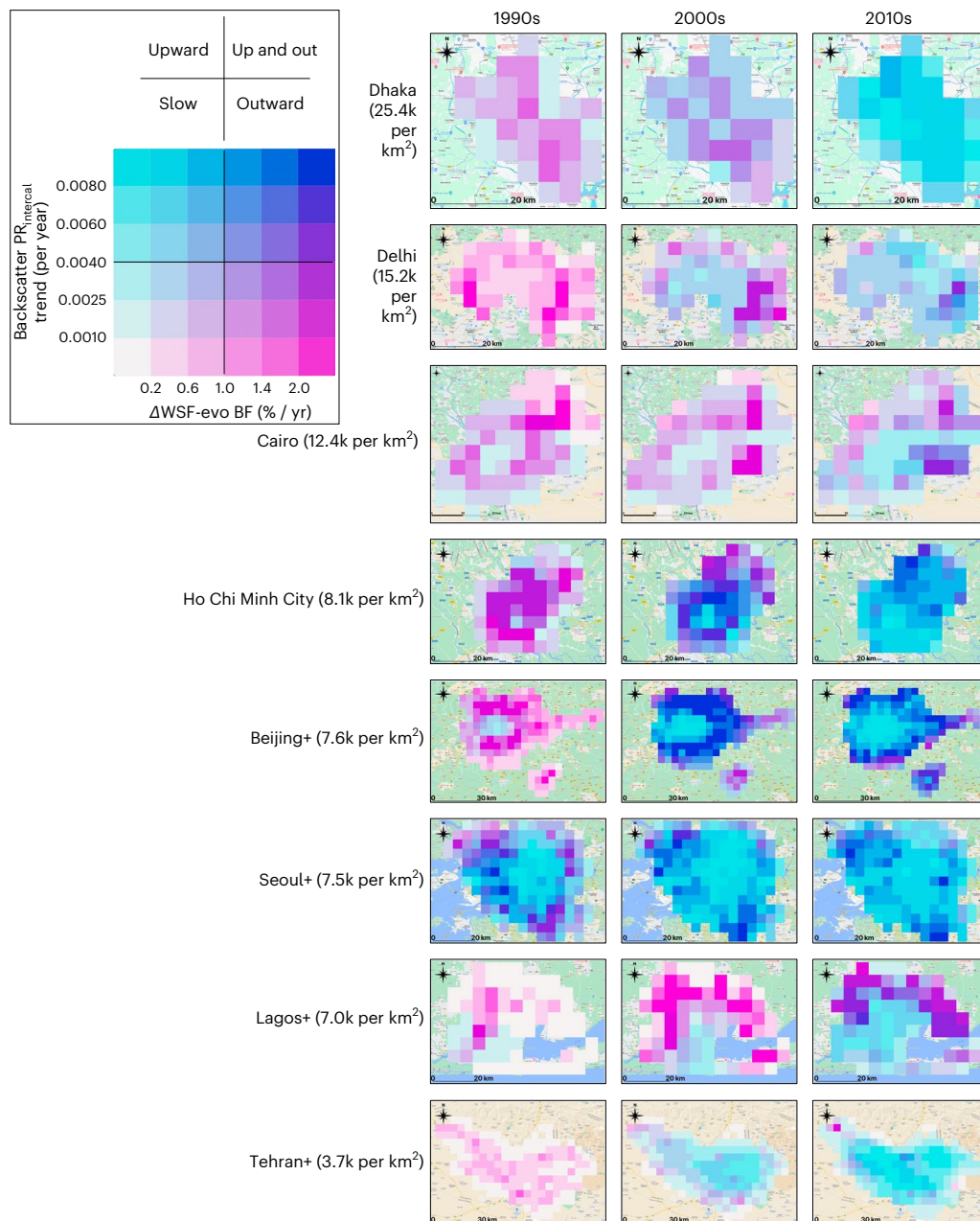


Fig. 1 | Bivariate plots of decadal urban BF and PR growth rates. Plots are shown at the 0.05° grid cell level, with three plots (left: 1990s; middle: 2000s; right: 2010s) for each of eight megacities (2014 population $>10\text{M}$) with the 2014 mean city population densities listed in parentheses. The rates are WSF-*evo* BF increase (percentage per year) for 1993–2000, 1999–2009 and 2010–2015, and backscatter PR trend (per year) for ERS (1993–2000), QSCAT (1999–2009) and

ASCAT (2010–2021), with each metric binned into six ranges. The 36 bivariate bins are grouped into four broad growth categories (legend). The Beijing+ maps include the smaller Langfang MUA to the southeast of Beijing. Background maps are included for context, not used for data. Map copyright 2022 Google. Map data copyright Google Roads.

to those identified in an earlier study⁸. In addition to the ‘fast-up-and-out typology’ of the 2000s and 2010s, the analysis identified a ‘slow-up-and-out’ typology in the 2010s. The fast-up-and-out category includes grid cells with moderate (2000s) or large (2010s) initial BF and PR, which then expanded very rapidly in both vertical and lateral dimensions during the decade (Table 2). One interpretation of this typology is that these are established urban areas with high land values, hence with high-rises. With increases in investments, jobs and in-migration, these urban areas need to develop more housing and commercial space, further fueling increases in land prices and more upward development.

In the 1990s, two clusters had very similar slow growth and low initial state BF and PR characteristics (‘budding’ and ‘budding2’),

and these mostly merged into a single ‘budding’ cluster in the 2000s (Fig. 4). A 1990s *k*-means analysis with four clusters essentially merged these two (Extended Data Fig. 5d). Across the decades, globally, the largest share of urban grid cells was in the ‘budding’ urban growth typologies, decreasing from 64% (1990s) to 55% (2000s) to 47% (2010s) (Fig. 4 and Table 2). The second largest share was the ‘stabilized’ cluster, with high BF and slow growth in BF and PR (Fig. 4 and Extended Data Fig. 5a–c). ‘Stabilized’ grid cells increased globally from 18% in the 1990s to 24% in the 2010s, mostly gaining ‘outward’ grid cells, while losing some to ‘slow-up-and-out’ and ‘upward’ (Fig. 4 and Extended Data Fig. 6). These slow-growth clusters dominated most regions, except East Asia (‘upward’ dominated in all three decades) and China

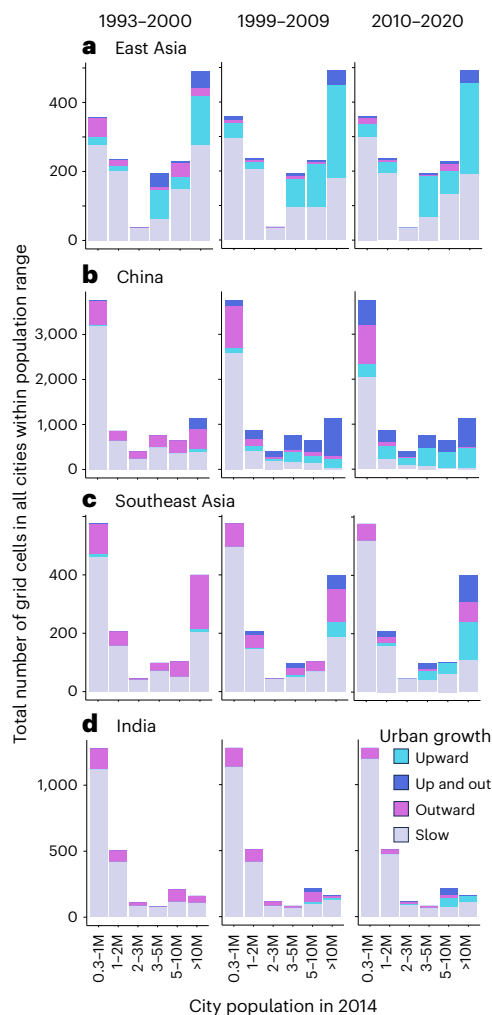


Fig. 2 | Regional variations in distribution in urban grid cell building growth rates by decade across eastern and southern Asia. a–d. Grid cell counts are plotted against city populations. For each region, East Asia (a), China (b), Southeast Asia (c) and India (d), cities are binned by total 2014 population (Taubenbock et al. 2019), and then the aggregated grid cells are partitioned into four urban growth rate classes; see legend in Fig. 1. Results for other regions are in Extended Data Fig. 3.

(‘slow-up-and-out’ in the 2010s) (Fig. 4 and Extended Data Fig. 6). The ‘outward’ typology was identified in the 1990s and 2000s, mostly in Asia and Africa; these grid cells mostly transition to ‘slow-up-and-out’, ‘fast-up-and-out’ and ‘stabilized’ in the 2010s.

Most of the fast-up-and-out grid cells in the 2000s and 2010s were in China (Fig. 4). By the 2010s, 6% of fast-up-and-out grid cells were in Africa (essentially all in West Africa), 5% in Southeast Asia and <3% in other regions. The slow-up-and-out typology occurred in the 1990s, particularly in East Asia, and in the 2010s, when it was present in most regions and had become the dominant typology in China. About 10% of the budding grid cells in the 1990s shifted to outward in the 2000s and two-thirds of these were in China (Fig. 4). About 15% of the 2000s budding cluster shifted to slow-up-and-out in the 2010s; this occurred in all regions, with >15% transitioning in China, East Asia, Southeast Asia and Russia, and <15% transitioning in other regions (Fig. 4 and Extended Data Fig. 6).

The upward growth typology, with large initial values of BF, fast upward and slow outward growth, was primarily in East Asia and Europe in the 1990s but declined there over time, transitioning to stabilized (that is, slower PR growth) (Fig. 4 and Extended Data Fig. 6). Meanwhile the upward typology had gains from the 2000s to 2010s

in China, mostly transitioning from slow-up-and-out, and smaller gains in Southeast Asia, other Asia, Africa, India and the Middle East (Fig. 4 and Extended Data Fig. 6).

Discussion

Two of the most widely held theories of urbanization are von Thünen’s model of land use²¹ and Burgess’s concentric zone model²². Although von Thünen’s model focused on agricultural land use and Burgess’s model focused on urban land use and social structures, they were conceptually very similar: intensity of land use radiates out from a core and is dependent on transport costs and accessibility as well as socioeconomic status. However, urbanization as a process of city or infrastructure development is under-theorized. This work shows, for the first time, that there is a city-building process (or process of infrastructure development) that undergoes distinct phases, corresponding with economic development¹⁹. Burgess’s model does not address built-up structure—it focuses on social structure. By combining data from many cities distributed across the world in different geographic regions, we show that this city-building process is both universal across regions and has distinct phases that occur in a particular sequence.

Types of urban built growth

Urban volumetric or 3D growth can arise from increases in building area or building height or both. Increasing BF represents land conversion from unbuilt to built-up; this could include construction of high-rise buildings meaning simultaneous horizontal and vertical expansion. Microwave backscatter is a direct measure that represents a change in land surface morphology, dielectric properties and orientation; in urban environments backscattering potential is mostly related to strong backscattering of dihedral corner reflectors (for example, exterior building walls and adjacent ground)^{16,17,23}. By combining completely independent BF and PR data, we infer four broad patterns of growth. One is slow growth, when rates of increase in BF and PR are both low; the other three patterns represent relatively rapid building growth: (1) outward, when the BF increase rate is high and that of PR low; (2) upward, when the PR increase rate is high and that of BF low; and (3) up-and-out growth, when BF and PR increase rates are both high, which could include lateral expansion and/or infilling (probably with taller buildings than before), along with replacement of shorter buildings by taller buildings.

Unbuilt land will have a BF value of zero, but unbuilt land’s PR magnitude is not zero—it will depend on vegetation type²⁴ and other surface characteristics¹⁷. Construction of scattered low-rise buildings on unbuilt land will increase BF, but may not increase PR substantially. Later in urban growth, as availability of unbuilt land area declines, rates of increase in BF may also decline, while backscatter PR can continue to increase if building volume continues to increase due to replacement of low-rise with high-rise buildings—for example, China, Shanghai+ and Beijing+ (Extended Data Fig. 2e–h). Heavy bombing damage in Syrian cities in the early 2010s²⁵ reduced PR (fewer intact, well-aligned dihedral corner reflectors; less building volume) without full recovery by 2020, but BF did not decline (Extended Data Fig. 7).

Trends in urban built growth

Two recent studies generated time series of 3D urban development from high-resolution SAR data, so far limited to a span of several years at a few metropolises^{10,11}. Recent global urban high-resolution 3D datasets have either been snapshots in time with no temporal change^{12–14} or used constant building heights coupled with annually changing BF²⁶, a simplifying but problematic assumption. A recent study combined Defense Meteorological Satellite Program and Visible Infrared Imaging Radiometer Suite nighttime light data to map the annually expanding edge of urban extent in Southeast Asia 1992–2018, but does not address 3D development²⁷. Our study presents a data-based measure of 3D urban change over multiple decades. Unlike earlier

Table 1 | Global and regional aggregate urban areas in four building growth rate classes for the 1990s, 2000s and 2010s. Areas in 1,000 km², rounded to nearest 100 km²; – implies an area of 0 (zero grid cells)

Region	1993–2000				1999–2009				2010–2021			
	Slow	Outward dominant	Upward dominant	Up-and-out	Slow	Outward dominant	Upward dominant	Up-and-out	Slow	Outward dominant	Upward dominant	Up-and-out
Global	710.4	145.1	25.0	11.7	680.0	106.5	50.3	55.3	661.4	64.0	99.4	67.4
Africa	72.3	11.0	2.6	0.8	72.8	13.2	0.7	–	69.0	8.7	5.5	3.5
Australia–New Zealand	10.7	1.9	–	–	11.5	1.0	0.2	–	11.0	0.7	0.8	0.1
China	135.9	50.7	1.9	6.8	90.6	36.2	20.1	48.4	64.5	26.7	49.5	54.7
East Asia	25.7	4.0	7.6	2.5	23.3	1.0	13.8	1.7	23.7	1.4	13.2	1.5
Europe	77.1	3.4	3.6	0.1	77.2	2.4	4.2	0.3	80.5	1.9	1.7	0.1
India	55.6	12.1	–	–	55.1	11.1	0.6	0.9	57.8	4.8	3.4	1.7
Latin America	83.8	14.1	7.9	1.4	98.4	7.5	1.0	0.2	102.6	3.5	0.9	0.1
Middle East	39.2	4.8	0.1	–	35.9	2.5	4.6	1.1	33.1	0.6	10.0	0.4
North America	125.9	21.7	1.0	<0.05	132.1	15.6	0.8	<0.05	143.0	3.3	2.2	0.1
Other Asia	30.1	7.3	–	–	30.9	5.1	1.1	0.4	30.0	2.4	4.2	0.9
Russia	24.0	1.3	–	–	21.9	1.6	1.6	0.1	17.7	5.3	1.8	0.5
Southeast Asia	30.1	12.8	0.5	0.1	30.3	9.3	1.6	2.2	28.6	4.7	6.2	4.0
Advanced economies	268.6	36.4	9.4	1.7	271.6	24.7	17.6	2.2	289.7	8.5	16.2	1.7
Other economies	441.9	108.6	15.6	10.0	408.4	81.8	32.8	53.1	371.7	55.5	83.2	65.7
Central Africa	10.1	0.6	0.3	–	10.1	0.7	0.2	–	9.8	0.5	0.6	–
Eastern Africa	11.6	2.8	1.6	0.3	14.1	2.3	–	–	13.1	1.2	1.9	0.2
Northern Africa	16.6	1.8	–	–	16.3	1.5	0.5	–	16.9	1.0	0.3	0.2
Southern Africa	7.9	1.1	0.7	0.5	9.6	0.5	–	–	10.0	0.1	–	–
Western Africa	26.3	4.6	–	–	22.7	8.2	–	–	19.3	5.9	2.6	3.1
Central Asia	18.9	4.3	–	–	19.1	3.1	0.8	0.2	17.7	1.5	3.3	0.7
Southern Asia	11.2	2.9	–	–	11.8	2.0	0.3	0.2	12.2	0.9	0.9	0.2

global studies assessing 3D growth over a single decade, for example⁸, the three decades of data show regionally varying accelerations and decelerations in rates of upward and outward growth and shifts in the dominant growth typology.

Much of the area of the 1,550+ large cities examined has been growing slowly during the 1990s through 2010s, in terms of both BF and PR growth metrics. This slow growth is occurring across the full range of BF, but rarely where values of PR are high. In most regions slow growth rates were less prevalent in larger cities (population >2M) than in smaller cities. In urban grid cells where building growth is moderate or rapid, there is a clear tendency for the dominant growth metric to shift from upward to outward, that is, from growing out to growing up, and this was more likely in more populous cities, consistent with more populous cities having more tall building height per kilometer square²⁸. This transition often first occurred in the central core of mega-cities, apparently independent of overall city population density, before spreading out toward the periphery; an exception to this pattern was Dhaka, the densest city.

Liu et al.²⁹ analyzed 30 years (1985–2015) of global urban (lateral) growth based on 30 m Landsat surface reflectance products, finding that global urban land area grew faster than global urban population, and that urban lateral growth rates were accelerating in Asia, Africa and South America, while decelerating in North America, Europe and Australia. Using this same dataset, Chakraborty et al.³⁰ found differences in horizontal growth patterns over the past few decades between large cities (>1M) in the Global North and the Global South, but acknowledged the limitation of ‘overlook(ing) the vertical aspect of urban expansion’. We found that outward growth was the dominant rapid growth category in the 1990s across all regions except East Asia and Europe; however, by the 2010s, it was not dominant in any region.

Overall, rapid upward growth was rare in the 1990s but increasingly common in the 2010s. Up-and-out growth was rare in the 1990s, but by the 2010s it was notable in China, Southeast Asia and Africa. While aggregate BF growth rates were decelerating in most regions over the 1990s to 2010s, except for accelerations in China and Africa (1990s to 2000s) and Russia (2000 to 2010s), PR growth rates were accelerating in many regions.

The lag in urban growth seen along the broad arc from East Asia through China and Southeast Asia to India (Fig. 2) is consistent with the timing of regional development across the area³¹. Overall, the multivariable spatiotemporal analysis provides a more complete and textured view of urban growth than analysis with either variable alone, and it leads to our observation that the growth of urban built-up areas has shifted from spreading out to building up over a period of a few decades, as BF growth rates decelerated while PR growth rates accelerated. As shown in previous studies, the dominant drivers of urban growth vary across the world, including factors such as population growth, governance and economic structure^{13,32}. The result of this multifactor forcing is that the rate and timing of the transition from lateral toward vertical growth varies across different regions and cities.

The fast-up-and-out urban growth typology identified in the 2000s and 2010s in this study highlights a unique urban upward growth, mostly found in Chinese cities and a consequence of the real estate boom there. Between 2003 and 2014, 100 billion square feet of residential real estate was constructed in Chinese cities³³. To put this into perspective, in 2018, total commercial real estate in the USA was 96 billion square feet (<https://www.eia.gov/cbecs>). However, as our results show, Chinese cities not only expanded in total volume, the fast-up-and-out typology indicates that there were many tall buildings constructed during this period. In 2017, 66% of the completed

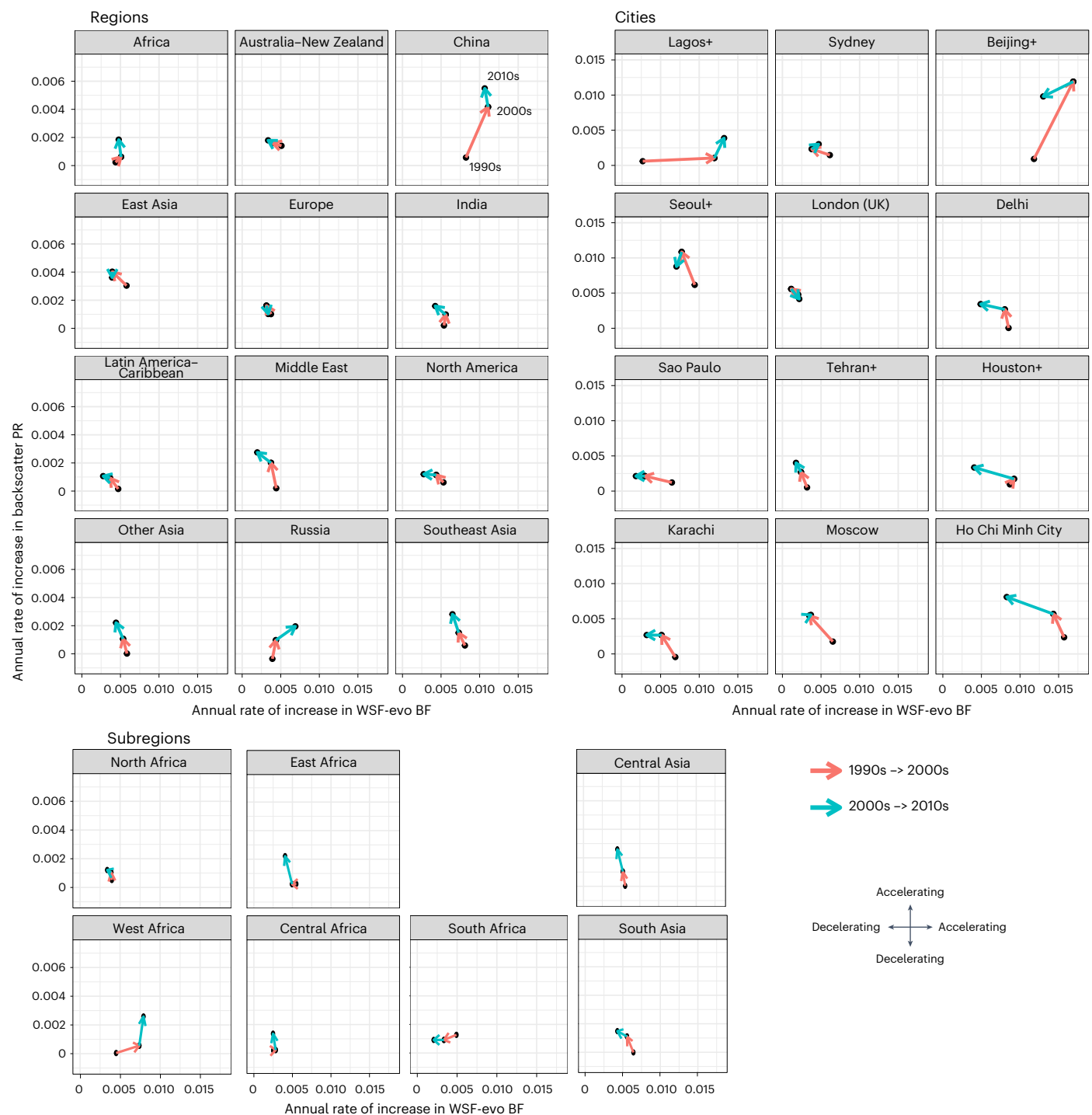


Fig. 3 | Trajectories of decadal changes in regional and city-building growth rates. Top left: decadal increases or decreases in growth rates of urban BF and urban backscatter (intercalibrated), aggregated across all grid cells in all MUAs of each of 12 regions. The black dots represent the mean growth rates of each decade (see China). The red arrows connect 1990s to 2000s growth rates; blue arrows connect 2000s to 2010s growth rates. Arrows pointing toward the right

(left) indicate accelerating (decelerating) growth rate in BF; arrows pointing upward (downward) indicate accelerating (decelerating) growth rate in PR. Bottom: same as top left but for subregions of Africa and Other Asia. Top right: same as top left but for an individual example city from each region. Note the y-axis scale is different in city graphs than in regional and subregional graphs.

skyscrapers worldwide that were 250 m or taller were built in China³⁴. The fast pace of skyscraper construction in China during this period is indicative of the rapid increase in land prices. Nationally, land prices doubled between 2000 and 2012 and tripled in some cities such as Beijing³⁵. Residential real estate prices increased even faster, by about four times during this period³⁵, leading a number of scholars to question whether China had a real estate bubble^{35,36}.

These global multidecadal data show large-scale patterns and trends, and can help test theories of economic development (for example, ref. 37). These results provide a longer spatiotemporal measure of a rate of accumulation of a substantial fraction of global physical capital (urban buildings) than other global remote sensing products so far. There is a general pattern over the three decades, outside ‘advanced-economy’ countries: the expansion of rapidly building urban land and

Table 2 | Total number of grid cells and characteristics of medians of global urban built environment *k*-means clusters by decade. See Extended Data Fig. 5a–c for the ranges of variable values in each cluster

Decade	No. grid cells (% total)	Growth typology	Cluster description	Amount		Rate	
				PR _{init}	BF _{init}	ΔPR/Δt	ΔBF/Δt
1990s	11,234 (32%)	Budding	Small area, moderate-rise, budding growth	Small	Small	Slow	Slow
	11,274 (32%)	Budding2	Small area, low-rise, budding growth	Small	Small	Slow	Slow
	6,342 (18%)	Stabilized	Large area, low-rise, stabilized growth	Small	Large	Slow	Slow
	3,723 (11%)	Outward	Medium area, low-rise, fast outward growth	Small	Medium	Slow	Fast
	2,307 (7%)	Upward	Medium area, high-rise, moderate upward growth	Large	Medium	Average	Slow
2000s	19,270 (55%)	Budding	Small area, low-rise, budding growth	Small	Small	Slow	Slow
	8,238 (24%)	Stabilized	Large area, mid-rise, stabilized growth	Medium	Large	Slow	Slow
	4,570 (13%)	Outward	Medium area, low-rise, fast outward growth	Small	Medium	Average	Fast
	1,230 (4%)	Fast-up-and-out	Medium area, mid-rise, fast upward and outward growth	Medium	Medium	Very fast	Very fast
	1,572 (5%)	Upward	Very large area, high-rise, fast upward growth	Very large	Very large	Fast	Slow
2010s	16,569 (48%)	Budding	Small area, low-rise, budding growth	Small	Small	Slow	Slow
	8,440 (24%)	Stabilized	Large area, mid-rise, stabilized growth	Medium	Large	Slow	Slow
	5,372 (16%)	Slow-up-and-out	Medium area, high-rise, slow upward and outward growth	Medium	Medium	Average	Average
	1,577 (5%)	Fast-up-and-out	Large area, high-rise, fast upward and outward growth	Large	Large	Very fast	Very fast
	2,562 (7%)	Upward	Very large area, high-rise, fast upward growth	Very large	Very large	Fast	Slow

the transition of this building growth from predominantly outward (low-rise) toward predominantly upward (high-rise), particularly in larger cities, which is consistent with a transition from a predominantly manufacturing toward a predominantly service economy in these large cities³⁸. Further analysis is needed, bringing in other data (for example, socioeconomic) but these results, independent from socioeconomic data, can indicate locations and time spans that could merit more detailed focus.

The data analyzed here can be useful for regional or global urban eco-environmental analyses, which often rely on coarse resolution data that is not uniformly collected or reported. A limitation noted in a recent study of 1970–2050 regional dynamics of building stock and construction material demand³⁹ was the model's sensitivity to assumptions and parameters based on a single study or data point, affecting detailed outcomes for specific regions or materials. A spatiotemporal dataset on 3D global urban growth could put a useful independent constraint on these types of global estimates of material use.

Limitations

A multidecadal backscatter time series requires data from different sensors, and there is an offset between sensor backscatter magnitude due to inherent wavelength and sensor differences for C-band (ERS and ASCAT) and Ku-band (QSCAT) scatterometers. As a result, it is challenging to assemble a reliable continuous annual time series of urban backscatter for three decades⁴⁰. To overcome this, we looked at each decade independently and computed intercalibrated decadal trends in backscatter for intercomparison. Owing to the range in slopes of the correlation between backscatter and building volume and height (Supplementary Fig. 2a,b), a universal conversion factor between these variables is unavailable, and quantitative intercomparisons between particular cities or regions is better focused on trends than on absolute magnitudes.

Backscatter data are coarse resolution, nominally ~5–10 km, so a detailed analysis of urban growth at the neighborhood scale in a particular city cannot be done, smaller cities are not good targets for analysis and the data are not suitable for disaster response efforts. In addition, this spatial resolution means that increasing backscatter in a single grid cell (~25 km²) of a growing city can be due to building volume growth that is a combination of new low buildings, new tall

buildings and replacement of low buildings with tall buildings. As a result, a globally generalizable interpretation of this signal is very difficult and the reference data (for example, lidar) to develop such an interpretation are not readily available across multiple cities and world regions and decades. However, this coarse spatial resolution also means that three decades of global annual urban backscatter data is not an unwieldy data volume.

Implications

The results presented in this study show that urban structural growth patterns across the world are evolving. Rapidly growing large cities in the twenty-first century are now mostly growing upward. The 2010s are more characterized by tall building development, with much more area in upward typologies in the 2010s (28%) than in the 2000s (9%) or the 1990s (7%). Historically, large-scale high-rise development was mostly limited to few megacities such as New York, Tokyo and Shanghai⁸. However, we have observed a shifting trend toward upward building growth across many cities and regions. Further focused analysis merging selected high-resolution SAR data from the three decades with backscatter and BF data could enhance our understanding of these changes.

This shift in growth has important positive and negative implications in terms of sustainable futures. Cities with taller built structure tend to have higher population densities, but these must be colocated with higher job densities to support public transportation to lower per capita emissions and create more walkability. Increasing population density alone is necessary, but insufficient for lowering transport emissions. Furthermore, the built environment does not need to be very tall to foster walkability; smaller block sizes are also important. Emissions aside, more land can be saved for nature with denser cities. However, very tall buildings have high embodied carbon and operational energy needs, require specialized materials and also create unique microclimates.

Methods

Experimental design

We modified the methodological approach from our two previously published papers^{7,8} on assessing urban growth in both upward and outward domains across global cities. The modifications are three-fold. Most importantly, we used a time series developed from a longer

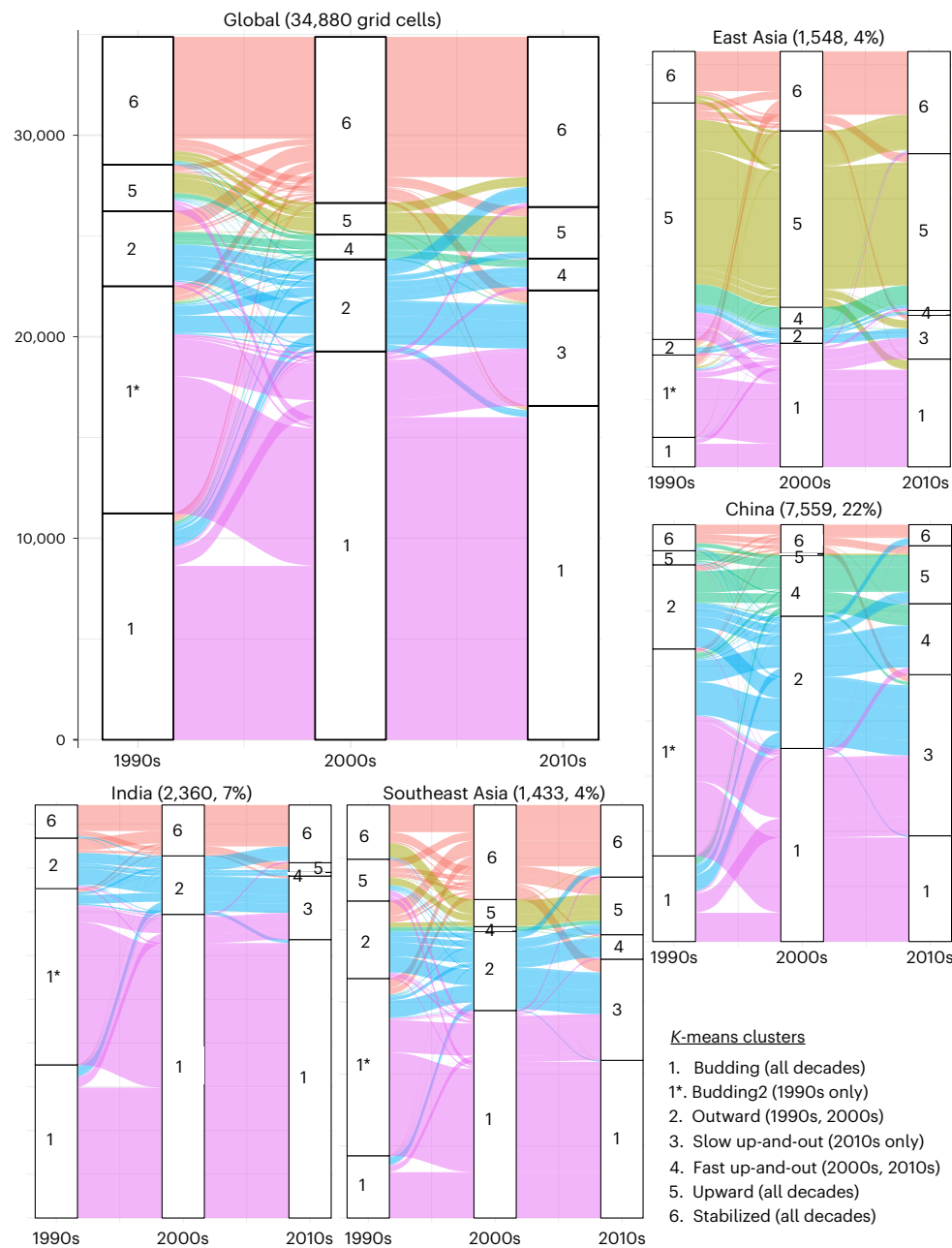


Fig. 4 | Interdecadal transitions in grid cell *k*-mean cluster classes. Top left: global urban grid cell transitions between clusters generated in the 1990s (left), 2000s (middle) and 2010s (right). Band widths are proportional to the number of grid cells transitioning from a cluster in one decade to a cluster in the next decade. Band colors are determined by the cluster identity in the 2000s. Right and bottom: the same as the global panel but for the subset of urban grid cells in each of four regions in Asia (the grid cell numbers per region as number and the

percent of global total listed after region names). Two clusters in the 1990s, 1 and 1*, have very similar characteristics (for cluster details, see Table 2 and Extended Data Fig. 5a–c) and mostly merge into a single budding cluster in the 2000s and 2010s. Note that not all clusters occur in all regions in all decades, for example, in the 2000s, India has urban grid cells in only three clusters (budding, outward and stabilized). Similar plots for other regions are in Extended Data Fig. 6 and for subregions in Supplementary Fig. 3.

record of backscatter data from three scatterometers, with a goal of understanding the dynamics of 3D urban growth over three decades. Second, we used a more rigorous definition of the urban domain and a larger number of cities. Finally, we used the WSF-evo dataset for measuring urban extent and outward growth (compared with nightlight and global human settlement layer BF data in earlier papers). Our spatial analysis covers global urban land on a 0.05° lat/lon grid. Our temporal analysis has annual time steps from 1993 to 2021, the period of available microwave backscatter data. We analyze and compare decadal trends, as this is the duration of individual scatterometer datasets and is long enough for observed trends to be important metrics of change.

Urban domain

In this study, we used global Morphological Urban Areas (MUAs)⁴¹ to define the spatial extent of 1,567 urban areas in 151 countries (Extended Data Table 1 and see Supplementary Information Table 1 for a full list of MUAs). In our earlier papers^{7,8}, city domains were defined by an 11×11 grid centered around the city core. That approach had issues of double counting of urban grid cells in adjacent cities and did not account for the actual shape of metropolitan regions (for example, Extended Data Fig. 8).

Taubenböck et al.⁴¹ identify some MUAs as an aggregation of several cities (for example, Los Angeles–Long Beach–Santa

Ana–Riverside–San Bernardino–Mission Viejo in the USA); to simplify notation we designate these by the first city name followed by a plus sign (for example, Los Angeles+; for a full list, see Supplementary Table 2). We overlaid all MUA polygons with a 0.05° lat/lon grid and identified all grid cells that were contained within or intersected an MUA polygon with that MUA (see the example in Extended Data Fig. 8). We also extracted MUA total population and polygon area data from this dataset; population was generated from United Nations data for 2014⁴¹. We computed MUA mean population density as the ratio of total (polygon) population to polygon area.

We excluded five MUAs for which we did not have either backscatter data (Honolulu, USA) or WSF-3D data (Al Ain, UAE; Hafar-al-Batin and Medina, Saudi Arabia; Zahedan, Iran). We then masked out all individual MUA grid cells with open water area $\geq 50\%$, using the Global 1-km Consensus Land Cover dataset⁴². After that, individual MUA size ranged from 389 grid cells (Guangzhou+, China) to one grid cell (Arkhangelsk, Russia). The total area of all 34,880 urban grid cells in our analysis is $\sim 890,000$ km², about 75% larger than the total area of all MUA polygons ($\sim 510,000$ km²) because all 0.05° lat/lon grid cells both within and intersecting the MUA polygon boundaries were included (see the example in Extended Data Fig. 8).

To summarize our global analysis, we aggregated many results to 12 global regions, and to illustrate the details at the MUA scale, we provide results for a single large city in each region (Extended Data Table 1). We also partitioned the Africa region into five subregions and the Other Asia region into two subregions (Extended Data Table 1).

WSF data

We aggregated the WSF-evo BF data for 1985–2015 (ref. 20) to 0.05° lat/lon (BF as fraction in range 0–1), and then extracted annual values for all MUA urban grid cells. For each grid cell, we computed annual rates of increase in BF at the grid cell level by ‘decade’ as $\Delta BF_{1990s} = (BF_{2000} - BF_{1993})/7$, $\Delta BF_{2000s} = (BF_{2009} - BF_{1999})/10$ and $\Delta BF_{2010s} = (BF_{2015} - BF_{2010})/5$.

We also aggregated the WSF-3D data¹² on building volume (as sum), building fraction (as mean) and building height (as mean) to a 0.05° lat/lon grid, using the same aggregation method as with WSF-evo data above, and then extracted values for all MUA urban grid cells. These data were not used for any temporal or change analyses presented here, but for a comparison of spatial patterns in 3D building metrics to backscatter across large cities. For comparison to ASCAT backscatter PR, these gridded WSF-3D data were smoothed with a 3×3 mean smoothing grid to more closely match the effective resolution of the ASCAT data⁴³. We chose the year of ASCAT data to compare with WSF-3D based on the best temporal match. WSF-3D building height represents 2012 status (based on TanDEM-X digital elevation model) and WSF-3D building fraction is defined by data from 2019 (it is independent from the WSF-evo product). WSF-3D building volume is the product of building height and building fraction and grid area, and so represents some hybrid of the urban state in 2012 and 2019; we chose 2015 ASCAT PR data for comparison to this 3D metric. We also compared annual time series of WSF-evo BF and ASCAT backscatter PR, 2007–2015, for Damascus, Aleppo and Homs in Syria, which were heavily bombed in the early 2010s²⁵.

Urban microwave backscatter data

We extracted summer season backscatter, σ° in dB, for all the MUA urban grid cells from a global 0.05° seasonal backscatter dataset covering 1993–2020 (ref. 44); see ref. 40 for dataset details. The summer season was designated as July–August–September for all grid cells in the Northern Hemisphere and January–February–March for all grid cells in the Southern Hemisphere. This backscatter annual time step data consists of data from three scatterometers: ERS (1993–2000), QuikSCAT or QSCAT (1999–2009) and ASCAT (2007–2020). We added an additional year of ASCAT backscatter σ° data (2021) to the time series,

using the same data source and processing as described in ref. 40. We converted backscatter in dB to power return ratio, PR ($=10^{(\sigma^\circ / 10)}$) for all analyses.

There is an offset in backscatter PR between the three sensors⁴⁰ (also see Extended Data Fig. 1), so we did not construct a continuous PR time series. To reduce impacts of short-term PR variability not likely to be due to urban development, we computed grid cell level annual backscatter trends (R command `lm`) separately for each sensor and decade: the 1990s: ERS (1993–2000); the 2000s: QuikSCAT (1999–2009 in the Northern Hemisphere, 2000–2009 in the Southern Hemisphere); and the 2010s: ASCAT (2010–2021). The sensor offset leads to a bias in annual trends, which is evident in the comparison of ASCAT and QSCAT trends for their three overlapping years of data, 2007–2009 (Extended Data Fig. 9a). To intercalibrate ASCAT to QSCAT, we scaled the ASCAT trends by the 2007–2009 mean QSCAT PR divided by the 2007–2009 mean ASCAT PR (Extended Data Fig. 9b). This grid cell level intercalibration factor was then applied to all ASCAT trends for the 2010s. Evaluating the ERS–QSCAT intercalibration is more problematic, as there are only 2 years of overlapping data for Northern Hemisphere cities (1999 and 2000) and only 1 year (2000) for Southern Hemisphere cities; 2-year ‘annual trends’ are just differences (with R^2 identically 1.0) and 1-year trends are undefined. Since most city-level backscatter PR trends were small in the 1990s (for example, Extended Data Fig. 1) a 2-year difference can be more noise than signal. We applied the same 3-year intercalibration method to ERS PR trends for the 1990s, that is, multiplying by the 1999–2001 QSCAT mean PR divided by the 1998–2000 ERS PR (using 2000–2002 mean QSCAT PR for the 12% of our target cities that are in the Southern Hemisphere (Extended Data Fig. 9c,d).

Building floor area data

In statistical datasets, building floor area is often computed as the building footprint times the number of stories in a building, and thus the floor area will be approximately proportional to the total building volume. We retrieved global building floor area data from online reports of the International Energy Agency (IEA). Specifically, we used the IEA global annual total floor area for 2000–2020 (<https://www.iea.org/data-and-statistics>) and this same global floor area for the years 2010, 2015, 2019, 2020 and 2021 but disaggregated into two subsets, ‘advanced economy’ countries and ‘emerging and developing economy’ countries (hereafter ‘other’ countries); country lists for this disaggregation come from IEA global energy analyses⁴⁵ and are listed in Extended Data Table 1.

We retrieved the national area of completed (new) building floor area for China for 1985–2021 (ref. 46). This national building footprint data was reported every 5 years from 1985 to 2005, and annually thereafter. We linearly interpolated between the 5-year reporting intervals before 2005 to get an estimate of annual new floor area. We also retrieved annual completed (new) building floor area for two municipalities: Beijing for 1990–2020 (ref. 47) and Shanghai for 1978–2019 (ref. 48). Since these national and municipal data represent only floor area of new completed buildings, with no information of total existing floor area, we computed accumulated new floor area for each region since the year before the particular data record begins, as a measure of increasing building volume at an annual time step. These datasets do not account for loss of floor area from demolition or restructuring of existing buildings.

Methodology

As backscatter strength is very sensitive to buildings as corner reflectors, construction of new buildings (infilling or lateral extension) or taller buildings can similarly influence backscatter. Therefore, we consider building volume, which would increase with either type of construction, to be the best proxy for backscatter strength, and combine the backscatter data with independent built fraction data to better discriminate different growth types.

We constructed annual time series of MUA-scale means of grid cell backscatter PR (1993–2021) and WSF-evo BF (1990–2015). Across the spatial variation of any large city, QSCAT backscatter has been shown to correlate with building height for nine US cities¹⁸. ASCAT backscatter PR has been shown to correlate with 2015 building volume estimates¹³ for China, Europe and the USA⁴⁰. We extended this analysis to global coverage, comparing 2012 ASCAT backscatter with WSF-3D building height, 2019 backscatter with WSF-3D building fraction and the mean of 2012 and 2019 backscatter with WSF-3D building volume, with WSF-3D data smoothed over 3×3 grids. Extended Data Fig. 9 shows these correlations for 12 MUAs, one per region.

To test whether temporal development in urban microwave PR and urban BF track temporal urban building growth, we computed aggregate annual microwave backscatter PR as the sum over all 0.05° urban MUA grid cells (1) globally, (2) in ‘advanced economy’ and ‘other economy’ countries, (3) in China, (4) in Beijing+ and (5) in Shanghai+, and compared these results with annual building floor area data (global and disaggregated into two ‘economies’) and to annual newly completed building floor area data (China, Beijing+ and Shanghai+). Similarly, we computed the mean annual WSF-evo BF for these same domains. We note that the IEA building floor area data is not restricted to urban domains, nor is the China new building floor area data, and that the Beijing and Shanghai statistical floor area data are for these municipality provinces, whose spatial extent does not fully align with the Beijing+ and Shanghai+ MUAs.

We constructed gridded maps of decadal bivariate trends in urban backscatter PR and WSF-evo BF. We then binned grid cells by their values of these decadal bivariate trends of MUA change into four broad categories: low or high rates of change (decadal trends) in backscatter PR coupled with low or high rates of change (decadal trends) in WSF-evo BF; these are (1) slow growth (low $\Delta PR/\Delta t$ and low $\Delta BF/\Delta t$), (2) area-dominant or outward growth (low $\Delta PR/\Delta t$ and high $\Delta BF/\Delta t$), (3) rapid 3D or up-and-out growth (high $\Delta PR/\Delta t$ and high $\Delta BF/\Delta t$) and (4) height-dominant or upward growth (high $\Delta PR/\Delta t$ and low $\Delta BF/\Delta t$), where t is time in years. We also quantified whether decadal growth rate trends in urban BF and PR accelerated or decelerated from the 1990s to the 2000s to the 2010s, aggregated at the regional scale and for individual MUAs.

Finally, we implemented a k -means analysis to group the global set of MUA grid cells into clusters. We used all MUA grid cells ($n = 34,880$), and performed separate, independent clustering for each decade, each based on the decade’s ‘initial state’ (for example, year 2000 QSCAT PR and WSF-evo BF) and growth rate (for example, mean annual rates of increase in QSCAT PR and WSF-evo BF in the 2000s). Since these clusters were generated for each decade independently, we use the actual PR values, not intercalibrated. Following ref. 8, we generated five clusters or typologies for each decade. We then identified which clusters had similar characteristics between decades and through this identified unique clusters across the three decades. Finally, we tracked grid cell trajectories from their 1990s typology to their 2000s typology to their 2010s typology, to study shifts and changes in urban growth over three decades at global and regional scales.

Reporting summary

Further information on research design is available in the Nature Portfolio Reporting Summary linked to this article.

Data availability

This study used published and publicly available data from several sources. The MUA polygons, polygon areas and 2014 populations are available as a link in the Supplementary Information to ref. 41. ERS, QSCAT and ASCAT seasonal urban backscatter data at 0.05° lat/lon resolution^{40,44} are available at the NASA Socioeconomic Data and Applications Center (<https://doi.org/10.7927/GR2E-DH86>). WSF-3D data (building height, volume and fraction cover¹²) are available at

<https://geoservice.dlr.de/web/maps/eoc:wsf3d>. WSF-evo data (settlement fractional cover by year, 1985–2015, ref. 20) are available at https://download.geoservice.dlr.de/WSF_EVO/. Building floor area data are available from the International Energy Agency (global totals data⁴⁵), the China Statistical Yearbook 2022 (ref. 46), the Beijing Statistical Yearbook 2021 (ref. 47) and the Shanghai Statistical Yearbook 2020 (ref. 48). MUA and WSF data were re-projected to 0.05° lat/lon grids (using Python 3.9.12, including Python packages numpy 1.22.3, pandas 1.4.2, rasterio 1.2.6, rioxarray 0.11.1, xarray 2022.3.0 and GDAL 3.31). Resulting tabular data at the 0.05° grid cell level that were analyzed in this study are provided as a supplementary plain text comma-separated variable file.

Code availability

Scripts used to generate the figures in this paper were developed in R-Studio (2022.07.2 Build 576, ‘Spotted Wakerobin’ Release (e7373ef8, 2022-09-06) for macOS). These scripts and the necessary input files are available via GitHub at https://github.com/sfrolking/Urban_three_decade_github_repo_final (ref. 49).

References

- Seto, K. C. et al. in *IPCC Climate Change 2014: Mitigation of Climate Change. Contribution of Working Group III to the Fifth Assessment Report of the Intergovernmental Panel on Climate Change* (eds Edenhofer, O. et al.) 923–1000 (Cambridge Univ. Press, 2014).
- The Weight of Cities: Resource Requirements of Future Urbanization* (International Resource Panel, United Nations Environment Programme, 2018).
- Oke, T. R. The energetic basis of the urban heat island. *Q. J. R. Meteorol. Soc.* **108**, 1–24 (1982).
- Schneider, A. & Woodcock, C. E. Compact, dispersed, fragmented, extensive? A comparison of urban growth in twenty-five global cities using remotely sensed data, pattern metrics and census information. *Urban Stud.* **45**, 659–692 (2008).
- Reba, M. & Seto, K. C. A systematic review and assessment of algorithms to detect, characterize and monitor urban land change. *Remote Sens. Environ.* **242**, 111739 (2020).
- Welch, R. Monitoring urban population and energy utilization patterns from satellite data. *Remote Sens. Environ.* **9**, 1–9 (1980).
- Frolking, S., Milliman, T., Seto, K. C. & Friedl, M. A. A global fingerprint of macro-scale changes in urban structure from 1999 to 2009. *Environ. Res. Lett.* **8**, 024004 (2013).
- Mahtta, R., Mahendra, A. & Seto, K. C. Building up or spreading out? Typologies of urban growth across 478 cities of 1 million+. *Environ. Res. Lett.* **14**, 124077 (2019).
- Balk, D. L., Nghiem, S. V., Jones, B. R., Liu, Z. & Dunn, G. Up and out: a multifaceted approach to characterizing urbanization in Greater Saigon, 2000–2009. *Landsc. Urban Plan.* **187**, 199–209 (2019).
- Che, M., Vizzello, A. & Gamba, P. Urban change pattern exploration of megacities using multitemporal nighttime light and Sentinel-1 SAR data. *IEEE J. Sel. Top. Appl. Earth Obs. Remote Sens.* **14**, 10681–10690 (2021).
- Che, M. & Gamba, P. Bi- and three-dimensional urban change detection using Sentinel-1 SAR temporal series. *Geoinformatica* **25**, 759–773 (2021).
- Esch, T. et al. World Settlement Footprint 3D—a first three-dimensional survey of the global building stock. *Remote Sens. Environ.* **270**, 112877 (2022).
- Li, M., Wang, Y., Rosier, J. F., Verburg, P. H. & van Vliet, J. Global maps of 3D built-up patterns for urban morphological analysis. *Int. J. Appl. Earth Obs. Geoinform.* **114**, 103048 (2022).
- Zhou, Y. et al. Satellite mapping of urban built-up heights reveals extreme infrastructure gaps and inequalities in the Global South. *Proc. Natl Acad. Sci. USA* **119**, e2214813119 (2022).

15. Wang, Y. et al. Characterizing annual dynamics of urban form at the horizontal and vertical dimensions using long-term Landsat time series data. *ISPRS J. Photogramm. Remote Sens.* **203**, 199–210 (2023).
16. Nghiem, S. V. et al. Observations of urban and suburban environments with global satellite scatterometer data. *ISPRS J. Photogramm. Remote Sens.* **64**, 367–380 (2009).
17. Ulaby, F. & Long, D. G. *Microwave Radar and Radiometric Remote Sensing* (Univ. Michigan Press, 2014).
18. Mathews, A. J., Frazier, A. E., Nghiem, S. V., Neumann, G. & Zhao, Y. Satellite scatterometer estimation of urban built-up volume: validation with airborne lidar data. *Int. J. Appl. Earth Obs. Geoinform.* **77**, 100–107 (2019).
19. Frolking, S., Mahtta, R., Milliman, T. & Seto, K. C. Three decades of global trends in urban microwave backscatter, building volume and city GDP. *Remote Sens. Environ.* **281**, 113225 (2022).
20. Marconcini, M. et al. Understanding current trends in global urbanisation—the world settlement footprint suite. *GI Forum_2021*, **1**, 33–38 (2021).
21. von Thünen, J. H. *The Isolated State: An English Edition of Der Isolierte Staat* (ed. Peter Geoffrey Hall) (Pergamon Press, Oxford, 1966).
22. Burgess, E. W. “The Growth of a City: An Introduction to a Research Project,” in *The City* (eds Park, R. E., Burgess, E. W. & McKennzie, R.) 47–62 (Univ. Chicago Press, 1925).
23. Paget, A. C., Frolking, S., Long, D. G. & Milliman, T. Satellite radar anisotropy observed in urban areas. *Int. J. Remote Sens.* **36**, 665–679 (2015).
24. Frolking, S. et al. Evaluation of the SeaWinds scatterometer for regional monitoring of vegetation phenology. *J. Geophys. Res. Atmos.* **111**, D17302 (2006).
25. Marx, A. J. Detecting urban destruction in Syria: a Landsat-based approach. *Remote Sens. Appl. Soc. Environ.* **4**, 30–36 (2016).
26. He, T. et al. Global 30 meters spatiotemporal 3D urban expansion dataset from 1990 to 2010. *Sci. Data* **10**, 321 (2023).
27. Zhao, M. et al. Mapping urban dynamics (1992–2018) in Southeast Asia using consistent nighttime light data from DMSP and VIIRS. *Remote Sens. Environ.* **248**, 111980 (2020).
28. Jedwab, R., Loungani, P. & Yezer, A. Comparing cities in developed and developing countries: population, land area, building height and crowding. *Reg. Sci. Urban Econ.* **86**, 103609 (2021).
29. Liu, X. et al. High-spatiotemporal-resolution mapping of global urban change from 1985 to 2015. *Nat. Sustain.* **3**, 564 (2020).
30. Chakraborty, S., Maity, I., Dadashpoor, H., Novotný, J. & Banerji, S. Building in or out? Examining urban expansion patterns and land use efficiency across the global sample of 466 cities with million-inhabitants. *Habitat Int.* **120**, 102503 (2022).
31. Chen, T.-L., Chiu, H.-W. & Lin, Y.-F. How do East and Southeast Asian cities differ from Western cities? A systematic review of the urban form characteristics. *Sustainability* **12**, 2423 (2020).
32. Mahtta, R. et al. Urban land expansion: the role of population and economic growth for 300+ cities. *NPJ Urban Sustain.* **2**, 5 (2022).
33. Glaeser, E., Huang, W., Ma, Y. & Shleifer, A. A real estate boom with Chinese characteristics. *J. Econ. Perspect.* **31**, 93–116 (2017).
34. Frolking, S. et al. Codes, input data files, and readme file for figures in Frolking et al. (2024) publication in Nature Cities. *GitHub* https://github.com/sfrolking/Urban_three_decade_github_repo_final (2024).
35. Zhao, S. X. B., Zhan, H., Jiang, Y. & Pan, W. How big is China's real estate bubble and why hasn't it burst yet? *Land Use Policy* **64**, 153–162 (2017).
36. Dreger, C. & Zhang, Y. Is there a bubble in the Chinese housing market? *Urban Policy Res.* **31**, 27–39 (2013).
37. Rostow, W. *The Stages of Economic Growth* (Cambridge Univ. Press, 1990).
38. Lall, S. et al. *Pancakes to Pyramids: City Form to Promote Sustainable Growth* (World Bank, 2021).
39. Deetman, S. et al. Modelling global material stocks and flows for residential and service sector buildings towards 2050. *J. Clean. Prod.* **245**, 118658 (2020).
40. Frolking, S. et al. A global urban microwave backscatter time series data set for 1993–2020 using ERS, QuikSCAT, and ASCAT data. *Sci. Data* **9**, 88 (2022).
41. Taubenböck, H. et al. A new ranking of the world's largest cities—do administrative units obscure morphological realities? *Remote Sens. Environ.* **232**, 111353 (2019).
42. Tuanmu, M.-N. & Jetz, W. A global 1-km consensus land-cover product for biodiversity and ecosystem modelling. *Glob. Ecol. Biogeogr.* **23**, 1031–1045 (2014).
43. Lindsley, R. D. & Long, D. G. Enhanced-resolution reconstruction of ASCAT backscatter measurements. *IEEE Trans. Geosci. Remote Sens.* **54**, 2589–2601 (2016).
44. Frolking, S. et al. Global monthly and seasonal urban and land backscatter time series, 1993–2020. *NASA Socioeconomic Data and Applications Center* <https://doi.org/10.7927/GR2E-DH86> (2022).
45. World energy outlook 2022. *IEA* <https://www.iea.org/reports/world-energy-outlook-2022> (2022).
46. China statistical yearbook 2022. *China Statistics Press* <http://www.stats.gov.cn/sj/ndsj/2022/indexeh.htm> (2022).
47. Beijing statistical yearbook 2021. *China Statistics Press, Beijing Municipal Bureau of Statistics and NBS Survey Office* <https://nj.tjj.beijing.gov.cn/nj/main/2021-tjnj/zk/indexeh.htm> (2021).
48. Shanghai statistical yearbook 2020. *Shanghai Municipal People's Government* <https://tj.sh.gov.cn/tjnj/zgsh/tjnj2020en.html> (2020).
49. Barr, J. & Luo, J. Growing skylines: the economic determinants of skyscrapers in China. *J. Real Estate Finance Econ.* **63**, 210–248 (2021).

Acknowledgements

We thank three anonymous reviewers for comments and suggestions that improved this manuscript. We thank J. Zeidler and M. Marconcini at DLR for help with processing the WSF-3D and WSF-evo data. The authors thank DLR for facilitating the research visit of T.E. to the World Bank in Washington, DC, USA, in 2022, which contributed to important improvements in the process of generating the WSF-3D data used in this study. Funding for this study was from: NASA Ocean Vector Winds Science Team program grant 80NSSC18K1434 (S.F. and T.M.); NASA Land Cover/Land Use Change program grant NNX15AD43G (K.C.S. and R.M.); European Space Agency contract no. 4000126100/19/I-EF (T.E.); and EU-funded ACP-EU Natural Disaster Risk Reduction Program, managed by the Global Facility for Disaster Reduction and Recovery of the World Bank, contract no. 7194331, contract no. 7196541 (T.E.).

Author contributions

Conceptualization, methodology, investigation and writing—original draft undertaken by S.F., R.M., T.M., T.E. and K.C.S. Visualization by S.F., R.M. and T.M. Input datasets by T.M. and T.E. Supervision and funding by S.F., K.C.S. and T.E. Writing—review and editing undertaken by S.F., R.M., T.E. and K.C.S.

Competing interests

The authors declare that they have no competing interests.

Additional information

Extended data is available for this paper at <https://doi.org/10.1038/s44284-024-00100-1>.

Supplementary information The online version contains supplementary material available at <https://doi.org/10.1038/s44284-024-00100-1>.

Correspondence and requests for materials should be addressed to Steve Frolking.

Peer review information *Nature Cities* thanks Bin Wu and the other, anonymous, reviewer(s) for their contribution to the peer review of this work.

Reprints and permissions information is available at www.nature.com/reprints.

Publisher's note Springer Nature remains neutral with regard to jurisdictional claims in published maps and institutional affiliations.

Open Access This article is licensed under a Creative Commons Attribution 4.0 International License, which permits use, sharing, adaptation, distribution and reproduction in any medium or format, as long as you give appropriate credit to the original author(s) and the source, provide a link to the Creative Commons licence, and indicate if changes were made. The images or other third party material in this article are included in the article's Creative Commons licence, unless indicated otherwise in a credit line to the material. If material is not included in the article's Creative Commons licence and your intended use is not permitted by statutory regulation or exceeds the permitted use, you will need to obtain permission directly from the copyright holder. To view a copy of this licence, visit <http://creativecommons.org/licenses/by/4.0/>.

© The Author(s) 2024

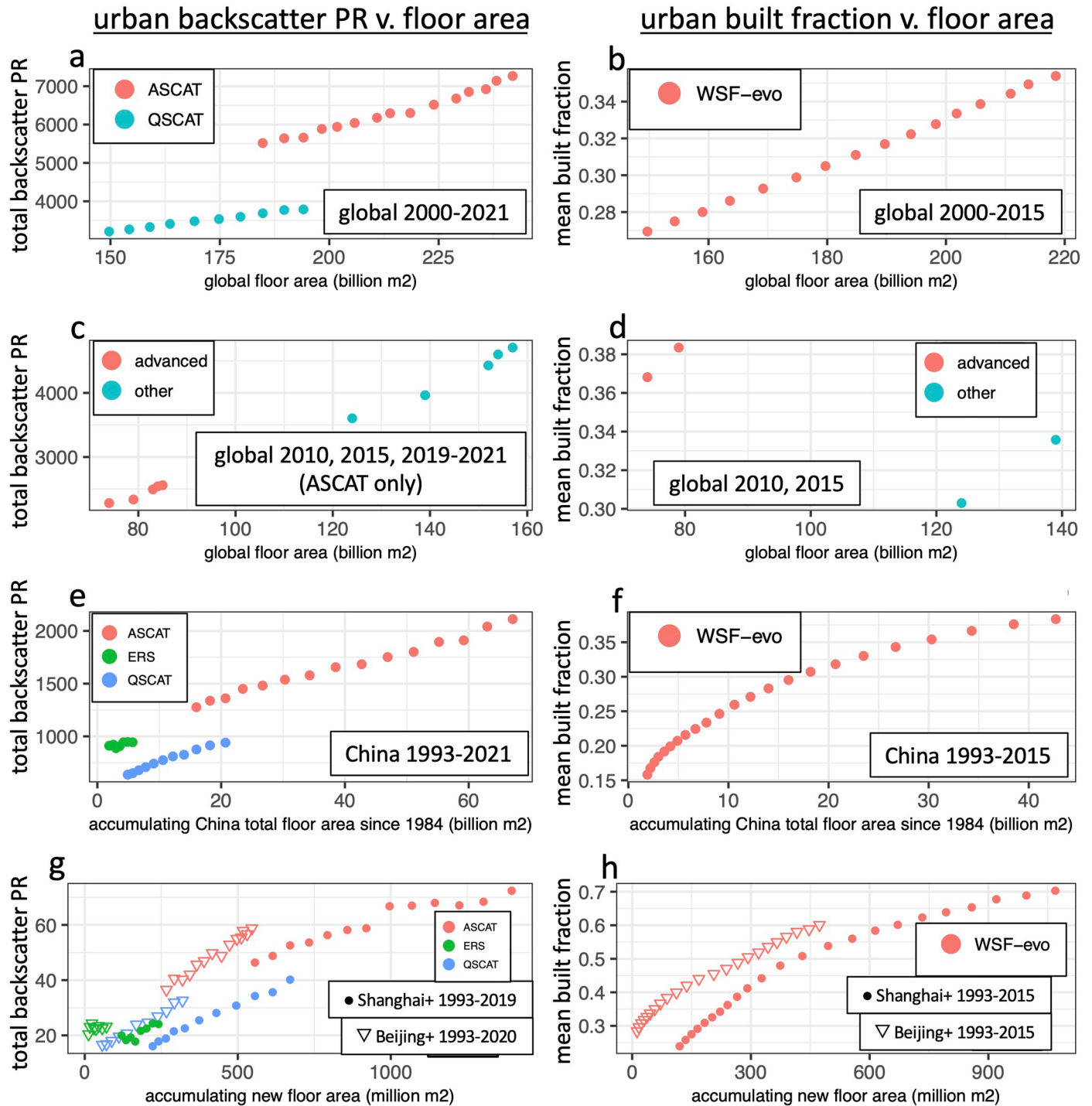
Extended Data Table 1 | List of 12 regions encompassing 151 countries included in the study

Region	Countries with at least one MUA	# grid cells	Example MUA
Africa	Algeria, Angola, Benin, Burkina Faso, Burundi, Cameroon, Central African Republic, Chad, Congo, Congo DRC, Djibouti, Egypt, Eritrea, Ethiopia, Gabon, Gambia, Ghana, Guinea, Guinea Bissau, Ivory Coast, Kenya, Liberia, Libya, Madagascar, Malawi, Mali, Mauritania, Morocco, Mozambique, Namibia, Niger, Nigeria, Rwanda, Senegal, Sierra Leone, Somalia, South Africa, South Sudan, Sudan, Tanzania, Togo, Tunisia, Uganda, Zambia, Zimbabwe	2974	Lagos+
AustraliaNZ	Australia, New Zealand	496	Sydney
China	China	7559	Beijing+
EastAsia	Hong Kong, Japan, Korea-North, Korea-South, Singapore, Taiwan	1549	Seoul+
Europe	Albania, Armenia, Austria, Belarus, Belgium, Bosnia Herzegovina, Bulgaria, Croatia, Czech Republic, Denmark, Estonia, Finland, France, Germany, Greece, Hungary, Ireland, Italy, Latvia, Lithuania, Macedonia, Moldova, Netherlands, Norway, Poland, Portugal, Romania, Serbia, Slovakia, Spain, Sweden, Switzerland, Ukraine, United Kingdom	4127	London
India	India	2360	Delhi
LatAmerCarib	Argentina, Bolivia, Brazil, Chile, Colombia, Costa Rica, Cuba, Dominican Republic, Ecuador, El Salvador, Guatemala, Haiti, Honduras, Jamaica, Mexico, Nicaragua, Panama, Paraguay, Peru, Puerto Rico, Uruguay, Venezuela	3714	Sao-Paulo
MiddleEast	Bahrain, Iran, Iraq, Israel, Jordan, Kuwait, Lebanon, Oman, Palestine, Qatar, Saudi Arabia, Syria, United Arab Emirates, Yemen	1659	Cairo
NorAmer	Canada, USA	6097	Houston+
OtherAsia	Afghanistan, Azerbaijan, Bangladesh, Georgia, Kazakhstan, Kyrgyzstan, Mongolia, Nepal, Pakistan, Sri Lanka, Tajikistan, Turkey, Turkmenistan, Uzbekistan	1518	Tashkent
Russia	Russia	1394	Moscow
SEAsia	Cambodia, Indonesia, Laos, Malaysia, Myanmar, Papua New Guinea, Philippines, Thailand, Viet Nam	1433	Ho-Chi-Minh-City
Sub-region			
North Africa	Algeria, Egypt, Libya, Morocco, Sudan, Tunisia,	690	—
East Africa	Burundi, Djibouti, Eritrea, Ethiopia, Kenya, Madagascar, Malawi, Mozambique, Rwanda, Somalia, South Sudan, Tanzania, Uganda, Zambia, Zimbabwe	543	—
West Africa	Benin, Burkina Faso, Gambia, Ghana, Guinea, Guinea Bissau, Ivory Coast, Liberia, Mali, Mauritania, Niger, Nigeria, Senegal, Sierra Leone, Togo	1011	—
Central Africa	Angola, Cameroon, Central African Republic, Chad, Congo, Congo DRC, Gabon	359	—
South Africa	Namibia, South Africa	371	—
Central Asia	Afghanistan, Azerbaijan, Georgia, Kazakhstan, Kyrgyzstan, Mongolia, Tajikistan, Turkey, Turkmenistan, Uzbekistan	997	—
South Asia	Bangladesh, Nepal, Pakistan, Sri Lanka	521	—

Study regions (that is, having at least one MUA), and 7 sub-regions of Africa and Other Asia, with total number of grid cells per region, and for each region a large city (MUA) that is used as example in some results. See Supplementary Information Table 1 for list of all MUAs.

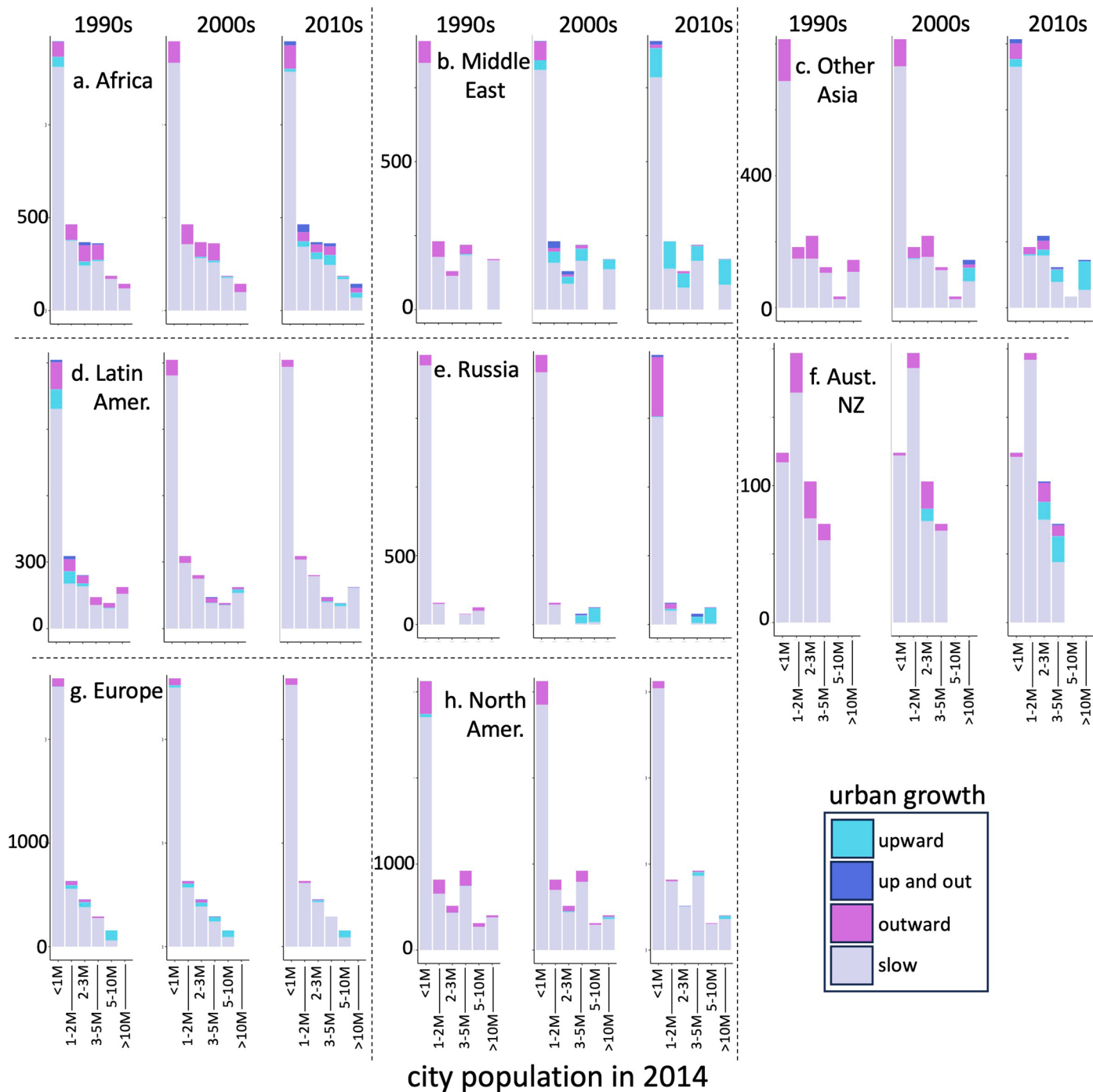


Extended Data Fig. 1 | Annual time series of backscatter and built fraction. *Left panels:* For each region, mean values of all urban grid-cells of summertime mean backscatter – ERS PR (1993–2000), QSCAT PR (1999–2009), ASCAT PR (2007–2021) – and WSF-evo built fraction (1990–2015). *Right panels:* as in left panels, but mean values of all grid cells in an example city for each region.



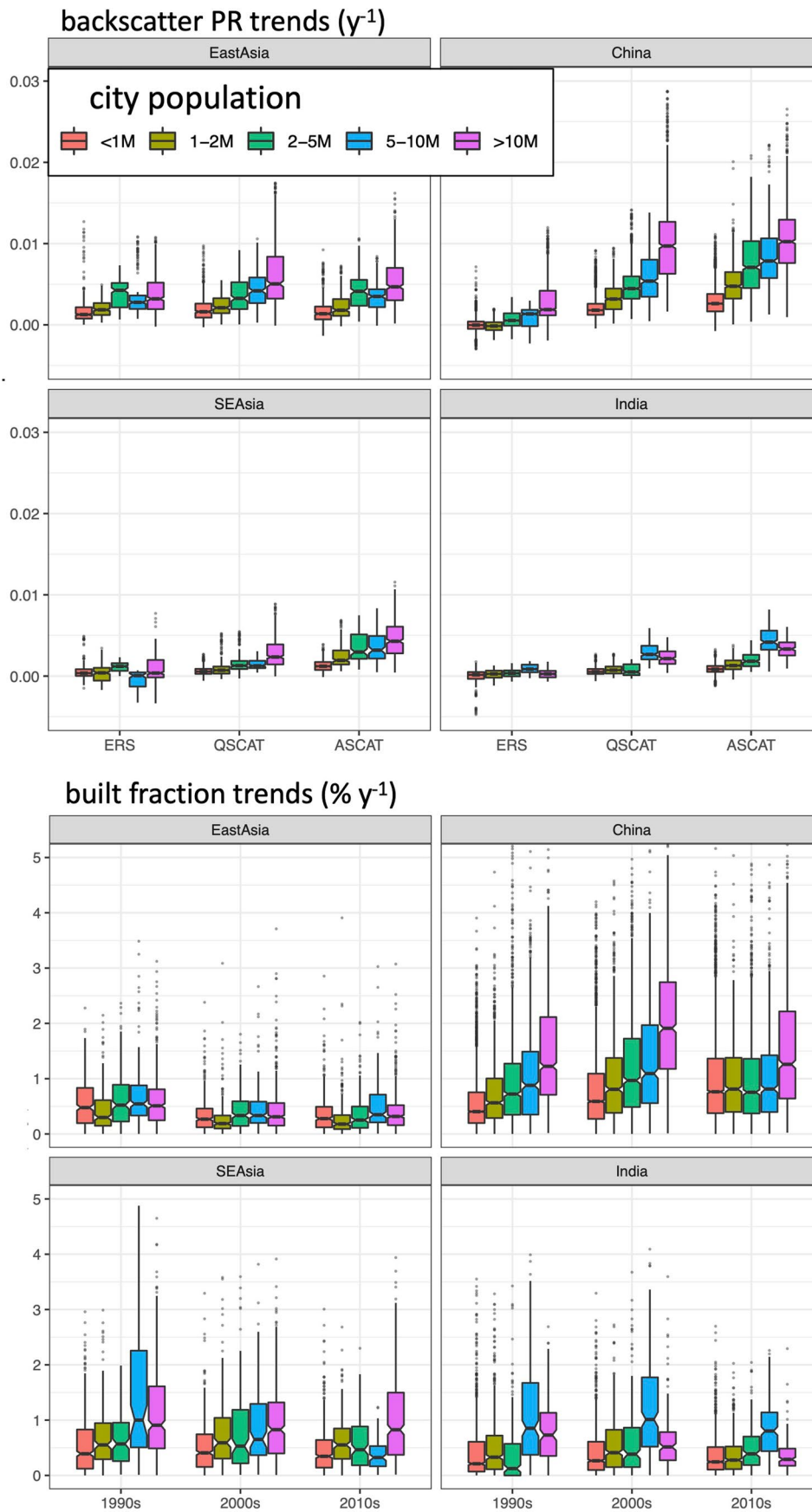
Extended Data Fig. 2 | Comparison of urban microwave backscatter PR (left column) and built fraction (right column) to independent estimates of building floor area. Global floor area compared to (a) aggregate backscatter for all urban MUA grid cells from QSCAT (2000–2009) and ASCAT (2007–2021), and (b) mean built fraction (2000–2015). (c, d) Subset of data from panels A and B disaggregated into countries with ‘advanced’ economies and with ‘developing and emerging’ (‘other’) economies; IEA floor area data for 2010, 2015, 2019, 2020, 2021. China annually accumulating new floor area since 1985 compared to (e) China’s MUA aggregated backscatter PR for ERS (1993–2000), QSCAT

(1999–2009), and ASCAT (2007–2021), and (f) mean urban built fraction across China’s 353 MUAs (1993–2015). Note that China floor area was linearly interpolated between reported data in 1990, 1995, 2000, 2005, but reported annually from 2005–2021. Annually accumulating new floor area for Beijing since 1989 and Shanghai since 1977 compared to (g) MUA aggregated backscatter PR for ERS (1993–2000), QSCAT (1999–2009), and ASCAT (2007–2020), and (h) mean built fraction (1993–2015). Note that x- and y-axis scales differ between the panels.



Extended Data Fig. 3 | Regional variations in frequency of urban grid cell growth rates by decade across eight global regions Regional variations in frequency of urban grid cell growth rates by decade across eight global regions not in eastern, southeastern or southern Asia plotted against city populations (see Fig. 2), (a) Africa, (b) Middle East, (c) Other Asia, (d) Latin America, (e) Russia,

(f) Australia-New Zealand, (g) Europe, and (h) North America. For each region, cities are binned by total 2014 population (Taubenbock et al. 2019) (ref. 41), and then the aggregated grid cells are partitioned into four urban growth rate classes (see Fig. 1 legend).

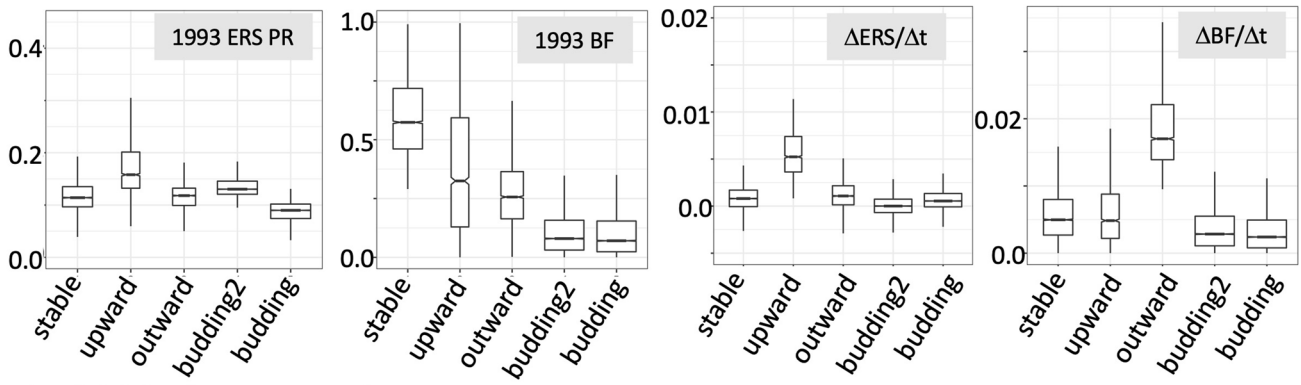


Extended Data Fig. 4 | See next page for caption.

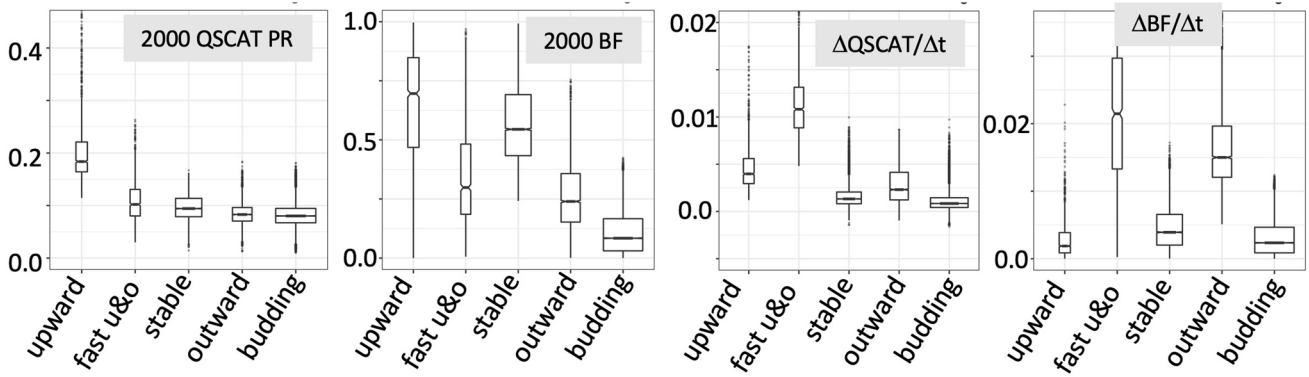
Extended Data Fig. 4 | Distribution of PR and BF trends by decade/sensor, binned by city population in 2014, for all cities in East Asia, China, Southeast Asia, and India. Number of cities per bin are: China: >10 M: 5 ($n = 1234$ total grid cells), 5–10 M: 9 ($n = 720$), 2–5 M: 26 ($n = 1217$), 1–2 M: 27 ($n = 959$), <1 M: 286 ($n = 3910$); East Asia: >10 M: 3 ($n = 539$), 5–10 M: 3 ($n = 255$), 2–5 M: 6 ($n = 292$), 1–2 M: 8 ($n = 278$), <1 M: 23 ($n = 420$); Southeast Asia: >10 M: 4 ($n = 432$), 5–10 M: 2

($n = 104$), 2–5 M: 5 ($n = 179$), 1–2 M: 11 ($n = 225$), <1 M: 53 ($n = 674$); and India: >10 M: 3 ($n = 181$), 5–10 M: 6 ($n = 234$), 2–5 M: 8 ($n = 210$), 1–2 M: 28 ($n = 538$), <1 M: 119 ($n = 1308$). Boxes: 50% of data centered on median; notches: -95% confidence intervals on median; whiskers: smaller of extreme value or 1.5 times length of inter-quartile range above and below median; dots: outliers.

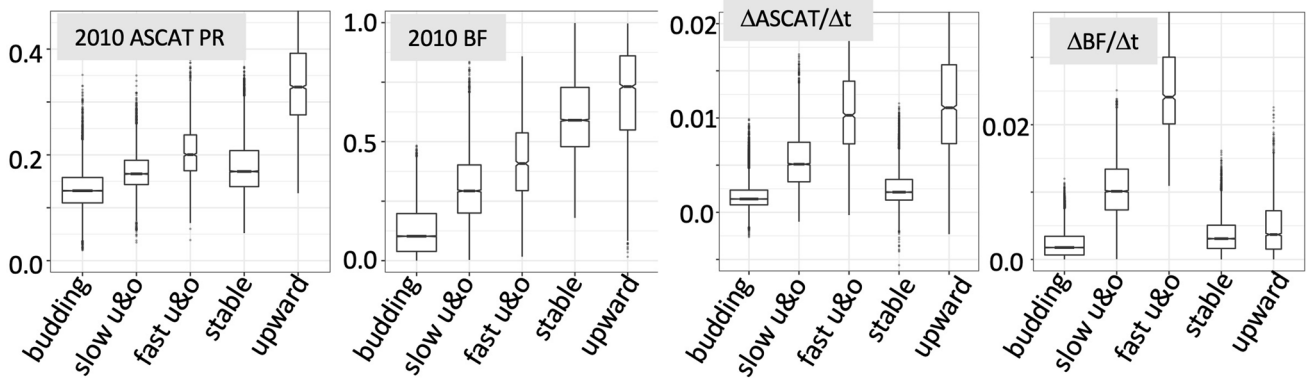
a. 1990s k-means clusters



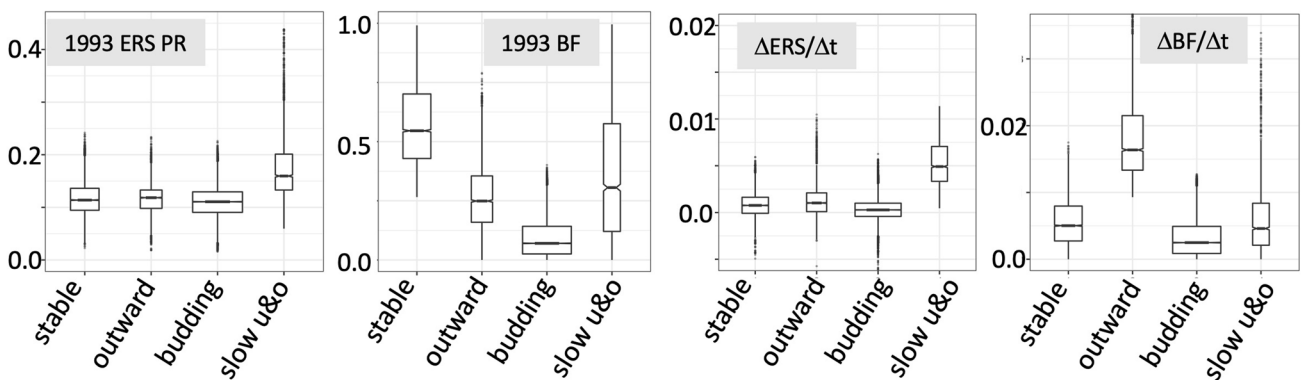
b. 2000s k-means clusters



c. 2010s k-means clusters



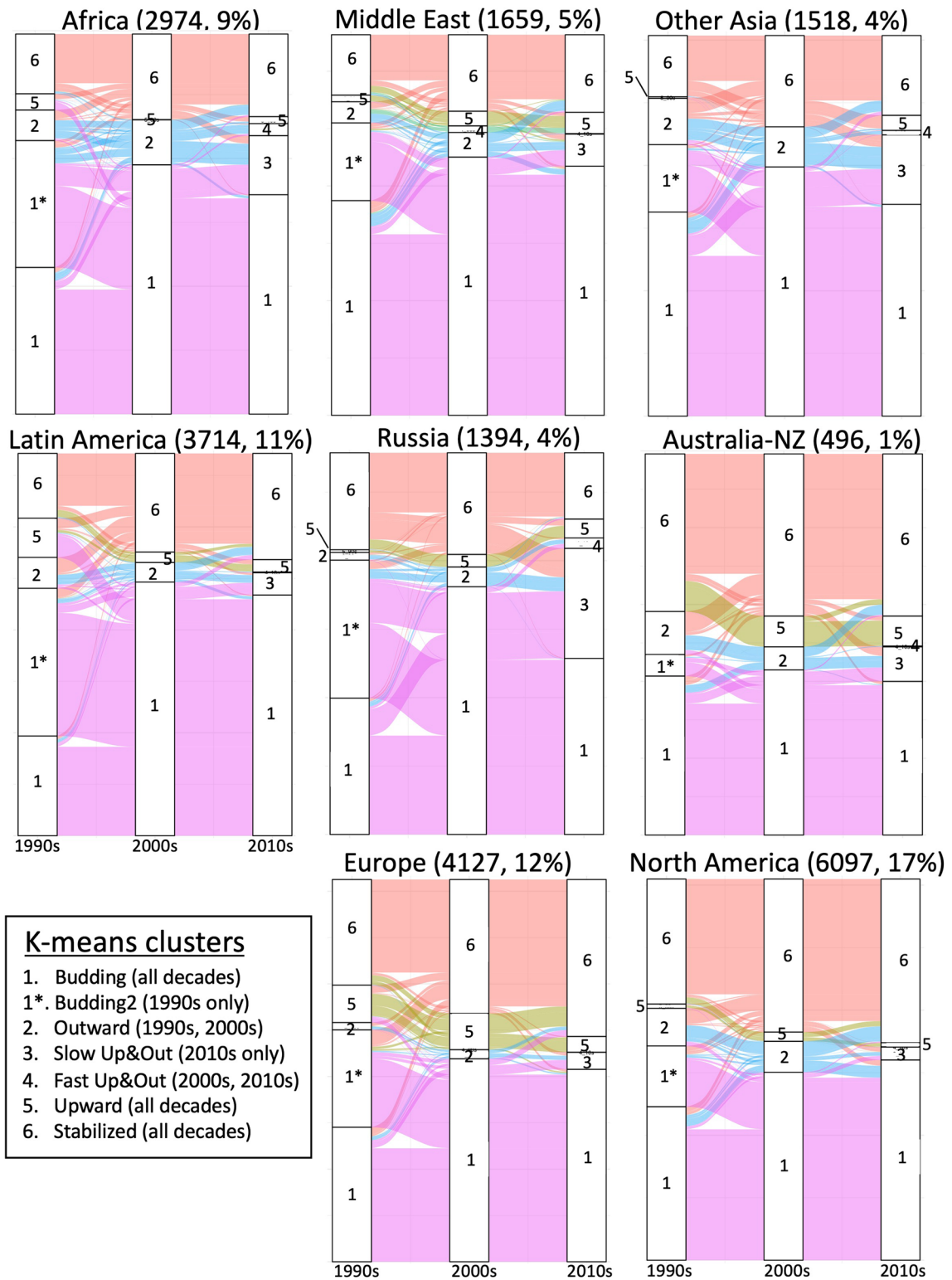
d. 1990s k-means FOUR clusters



Extended Data Fig. 5 | See next page for caption.

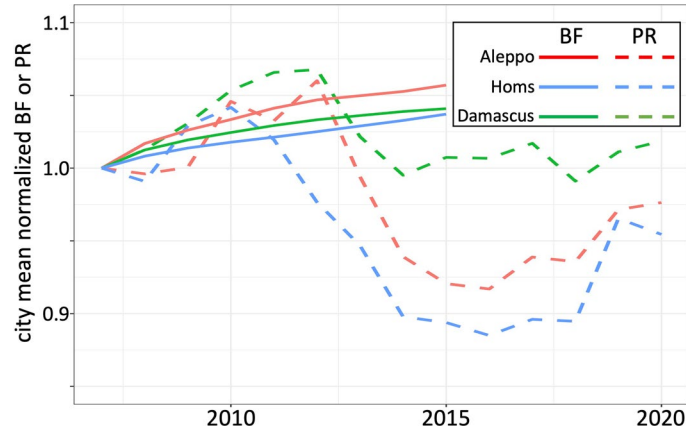
Extended Data Fig. 5 | Distribution of BF and PR initial states and rates of change in k-means clusters for each decade. All four cluster analyses included relevant data for 34,880 grid cells. **(a)** Five 1990s clusters, based on 1993 BF, 1993 ERS PR, 1993–2000 annual rate of increase in BF and annual trend in ERS PR. **(b)** Five 2000s clusters, based on 2000 BF, 2000 QSCAT PR, 1999–2009 annual rate of increase in BF and annual trend in QSCAT PR. **(c)** Five 2010s clusters, based on 2010 BF, 2010 ASCAT PR, 2010–2015 annual rate of increase in BF and

2010–2021 annual trend in ASCAT PR. **(d)** Four 1990s k-means clusters (not used in analysis). Boxes: inter-quartile range (that is, 50% of data centered on median); notches: approximate 95% confidence intervals on the median; whiskers (outer lines) extend to smaller of extreme value or 1.5 times length of inter-quartile range above and below the median. Outliers are shown as dots. Box widths are proportional to square root of number of grid cells in cluster. See Table 2 for more characterization of the k-means clusters.

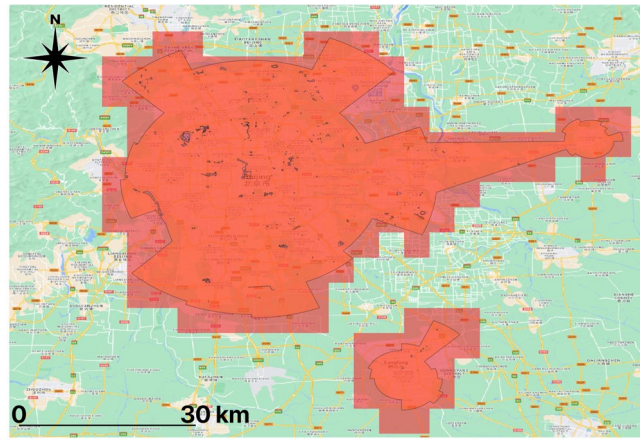


Extended Data Fig. 6 | Interdecadal transitions in grid cell k-mean clusters across eight global regions not in eastern, southeastern or southern Asia. MUA grid cell transitions (see Fig. 4) between clusters generated in the 1990s (left), 2000s (middle) and 2010s (right) for Africa, Middle East, Other Asia, Latin America, Russia, Australia-New Zealand, Europe, and North America. Number of grid cells per region and percentage of global total are listed in parentheses.

Band widths are proportional to the number of grid cells transitioning from a cluster in one decade to a cluster in the next decade. Band colors are determined by the cluster identity in the 2000s. Two clusters in the 1990s, 1 and 1*, have very similar characteristics (see Table 2 for cluster details) and merge into a single *Budding* cluster in the 2000s and 2010s. Note that not all clusters occur in all regions in all decades.

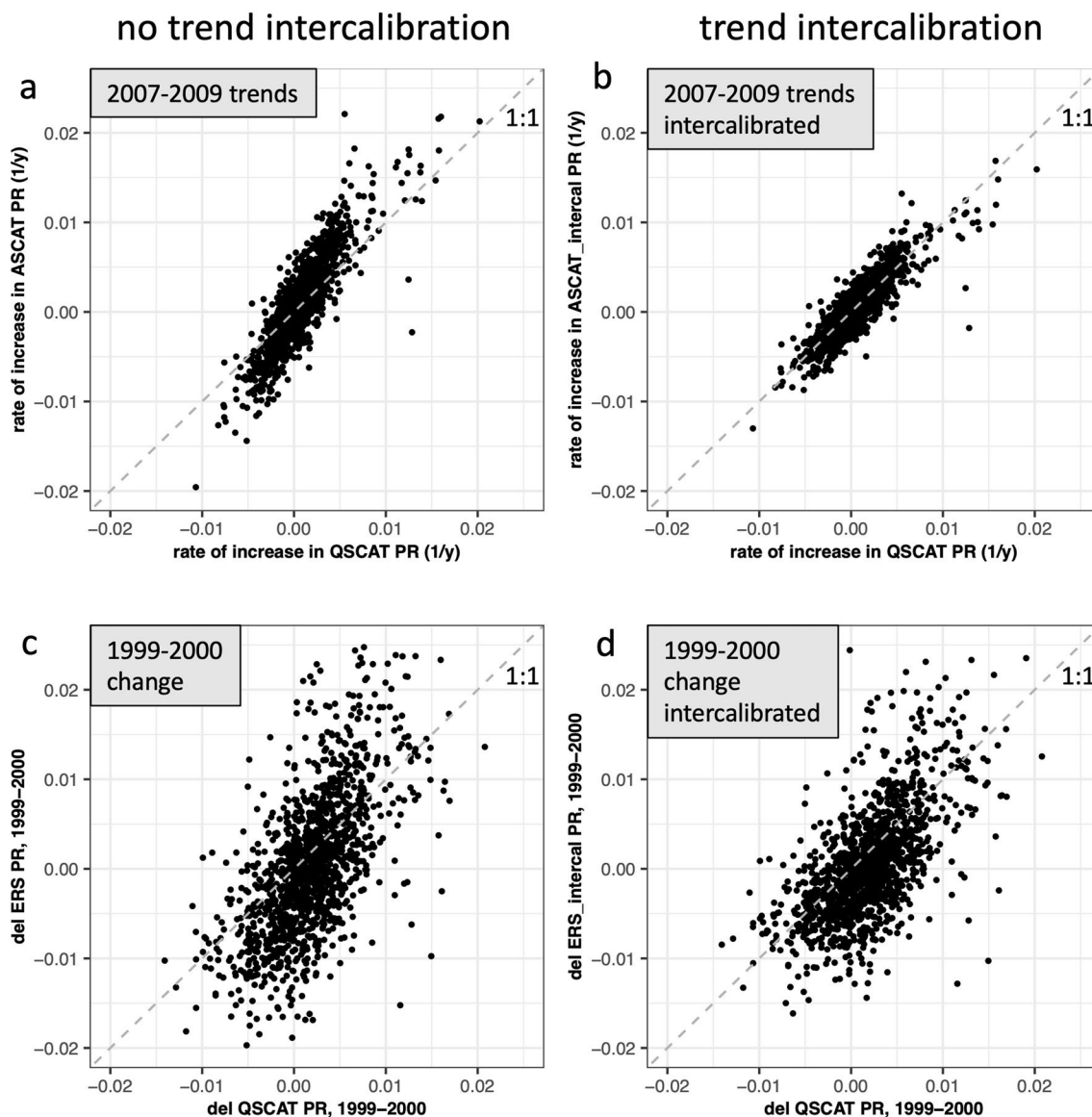


Extended Data Fig. 7 | Mean annual WSF-evo BF and ASCAT PR values for three cities in Syria, relative to 2007 values. These cities were heavily damaged by bombing in the early 2010s.



Extended Data Fig. 8 | Map of Beijing, China region. Beijing+ MUA polygon (red) from Taubenböck et al. (2019) (ref. 40). The grid cells (pale red, 0.05° lat/lon) that intersect the MUA polygon are included in the analysis. This map also

includes the MUA polygon and grid cells for the smaller MUA of Langfang, China, to the southeast of Beijing+. Background map included for context, not used for data; Map © 2022 Google, Map Data © Google Roads.



Extended Data Fig. 9 | Backscatter sensor trend intercalibrations.

(a) City-scale mean QSCAT and ASCAT three-year PR trends for 2007–2009. (b) QSCAT:ASCAT sensor intercalibration adjusts ASCAT trend by ratio of mean QSCAT PR to ASCAT PR for 2007–2009. (c) QSCAT and ERS 2-year PR differences (2000 minus 1999) for northern hemisphere cities only; southern hemisphere cities had no summer mean QSCAT data for 1999, so there is only one year of

overlap. (d) QSCAT:ERS sensor intercalibration adjusts ERS trend by ratio of mean QSCAT PR (1999–2001 for northern hemisphere cities, 2000–2002 for southern hemisphere cities) to ERS PR (1998–2000). Southern hemisphere cities had the QSCAT:ERS PR intercalibration applied for analysis in the paper, but are not plotted here as trends cannot be intercompared with only one year of common data. Dashed lines are 1:1.

Reporting Summary

Nature Portfolio wishes to improve the reproducibility of the work that we publish. This form provides structure for consistency and transparency in reporting. For further information on Nature Portfolio policies, see our [Editorial Policies](#) and the [Editorial Policy Checklist](#).

Statistics

For all statistical analyses, confirm that the following items are present in the figure legend, table legend, main text, or Methods section.

- | n/a | Confirmed |
|-------------------------------------|--|
| <input type="checkbox"/> | <input checked="" type="checkbox"/> The exact sample size (n) for each experimental group/condition, given as a discrete number and unit of measurement |
| <input type="checkbox"/> | <input checked="" type="checkbox"/> A statement on whether measurements were taken from distinct samples or whether the same sample was measured repeatedly |
| <input type="checkbox"/> | <input checked="" type="checkbox"/> The statistical test(s) used AND whether they are one- or two-sided
<i>Only common tests should be described solely by name; describe more complex techniques in the Methods section.</i> |
| <input checked="" type="checkbox"/> | <input type="checkbox"/> A description of all covariates tested |
| <input checked="" type="checkbox"/> | <input type="checkbox"/> A description of any assumptions or corrections, such as tests of normality and adjustment for multiple comparisons |
| <input type="checkbox"/> | <input checked="" type="checkbox"/> A full description of the statistical parameters including central tendency (e.g. means) or other basic estimates (e.g. regression coefficient) AND variation (e.g. standard deviation) or associated estimates of uncertainty (e.g. confidence intervals) |
| <input checked="" type="checkbox"/> | <input type="checkbox"/> For null hypothesis testing, the test statistic (e.g. F , t , r) with confidence intervals, effect sizes, degrees of freedom and P value noted
<i>Give P values as exact values whenever suitable.</i> |
| <input checked="" type="checkbox"/> | <input type="checkbox"/> For Bayesian analysis, information on the choice of priors and Markov chain Monte Carlo settings |
| <input checked="" type="checkbox"/> | <input type="checkbox"/> For hierarchical and complex designs, identification of the appropriate level for tests and full reporting of outcomes |
| <input checked="" type="checkbox"/> | <input type="checkbox"/> Estimates of effect sizes (e.g. Cohen's d , Pearson's r), indicating how they were calculated |

Our web collection on [statistics for biologists](#) contains articles on many of the points above.

Software and code

Policy information about [availability of computer code](#)

- | | |
|-----------------|--|
| Data collection | Data were all acquired from open source data repositories, details in Data Availability section and references (and also below): backscatter from NASA SEDAC, building footprint from World Settlement Footprint (DRL), floor area from IEA and China, Beijing, and Shanghai Statistical Yearbook, MUA data from Tubenbock et al. (2019 supplementary data). These data were either available at or were reprojected to a common 0.05 degree latitude longitude grid using python 3.9.12 (including python packages numpy 1.22.3, pandas 1.4.2, rasterio 1.2.6, rioarray 0.11.1, xarray 2022.3.0) and GDAL 3.31. |
| Data analysis | Scripts used to generate the figures in this paper were developed in R-Studio (2022.07.2 Build 576, "Spotted Wakerobin" Release (e7373ef8, 2022-09-06) for macOS). These scripts and the necessary input files are available at https://github.com/sfrolking/Urban_three_decade_github_repo_final . |

For manuscripts utilizing custom algorithms or software that are central to the research but not yet described in published literature, software must be made available to editors and reviewers. We strongly encourage code deposition in a community repository (e.g. GitHub). See the Nature Portfolio [guidelines for submitting code & software](#) for further information.

Data

Policy information about [availability of data](#)

All manuscripts must include a [data availability statement](#). This statement should provide the following information, where applicable:

- Accession codes, unique identifiers, or web links for publicly available datasets
- A description of any restrictions on data availability
- For clinical datasets or third party data, please ensure that the statement adheres to our [policy](#)

This study used published and publicly available data from several sources. The MUA polygons, polygon areas, and 2014 populations are available as a link in the Supplementary Material to Reference (40, Taubenbock et al. 2019, <https://doi.org/10.1016/j.rse.2019.111353>). ERS, QSCAT and ASCAT seasonal urban backscatter data at 0.05° lat/lon resolution (39, 44) are available at the NASA Socioeconomic Data and Applications Center (doi: doi:10.7927/GR2E-DH86). World Settlement Footprint 3D data (building height, volume, and fraction cover; ref. (12)) are available at <https://download.geoservice.dlr.de/WSF3D/files/>. World Settlement Footprint Evolution data (settlement fractional cover by year, 1985-2015, ref. (42)) are available at https://download.geoservice.dlr.de/WSF_EVO/. Building floor area data are available from the International Energy Agency (global totals data, Ref. (45, <https://www.iea.org/reports/world-energy-outlook-2022>)), the China Statistical Yearbook 2022 (46, <http://www.stats.gov.cn/sj/ndsj/2022/indexh.htm>), the Beijing Statistical Yearbook 2021 (47, <https://nj.tj.beijing.gov.cn/nj/main/2021-tjn/zk/indexh.htm>), and the Shanghai Statistical Yearbook 2020 (48, <https://tj.sh.gov.cn/tjn/zgsh/tjn2020en.html>). MUA and World Settlement Footprint data were re-projected to 0.05° lat/lon grids (using python 3.9.12, including python packages numpy 1.22.3, pandas 1.4.2, rasterio 1.2.6, rioarray 0.11.1, xarray 2022.3.0, and GDAL 3.3.1). Resulting tabular data at the 0.05° grid cell level that were analyzed in this study are provided as a supplementary plain text comma-separated variable file.

Research involving human participants, their data, or biological material

Policy information about studies with [human participants or human data](#). See also policy information about [sex, gender \(identity/presentation\), and sexual orientation](#) and [race, ethnicity and racism](#).

Reporting on sex and gender

Reporting on race, ethnicity, or other socially relevant groupings

Population characteristics

Recruitment

Ethics oversight

Note that full information on the approval of the study protocol must also be provided in the manuscript.

Field-specific reporting

Please select the one below that is the best fit for your research. If you are not sure, read the appropriate sections before making your selection.

Life sciences Behavioural & social sciences Ecological, evolutionary & environmental sciences

For a reference copy of the document with all sections, see [nature.com/documents/nr-reporting-summary-flat.pdf](https://www.nature.com/documents/nr-reporting-summary-flat.pdf)

Ecological, evolutionary & environmental sciences study design

All studies must disclose on these points even when the disclosure is negative.

Study description	Study presents analysis of multi-decadal global urban remote sensing data of built fraction and microwave backscatter, to look at rates and changes in rates in urban 3-D growth.
Research sample	Research 'samples' are ~1550 cities globally, their domain (extent) defined by another study as reported in methods. For each grid cell in each city, there is an annual time series of microwave backscatter and Landsat-derived built fraction; details in Methods section.
Sampling strategy	all data were included in the analysis.
Data collection	We downloaded publicly available data (urban seasonal microwave backscatter, World Settlement Footprint built fraction (WSF-evolution) and 3D data, city or Morphological Urban Area (MUA) extent polygon and populations; details in Methods section.
Timing and spatial scale	Spatial extent: global cities (~1550), city extents from Taubenbock et al. (2019) polygon data. Spatial scale: 0.05° lat/lon grids. Total of 34,880 urban grid cells. Temporal scale: annual WSF built fraction 1993-2015; annual (summer mean) microwave backscatter: ERS (1993-2000), QSCAT (1999-2009), and ASCAT (2007-2021).

Data exclusions	As described in Methods, data were excluded for six cities that did not have complete data from all sources (microwave backscatter, WSF-evolution, WSF-3D).
Reproducibility	Data analysis only, so reproducible with publicly available data.
Randomization	not relevant, as only groupings of data were identified geographic regions (e.g., North America, not random), or individual cities (e.g., Beijing, not random).
Blinding	not applicable
Did the study involve field work?	<input type="checkbox"/> Yes <input checked="" type="checkbox"/> No

Reporting for specific materials, systems and methods

We require information from authors about some types of materials, experimental systems and methods used in many studies. Here, indicate whether each material, system or method listed is relevant to your study. If you are not sure if a list item applies to your research, read the appropriate section before selecting a response.

Materials & experimental systems

n/a	Involvement in the study
<input checked="" type="checkbox"/>	<input type="checkbox"/> Antibodies
<input checked="" type="checkbox"/>	<input type="checkbox"/> Eukaryotic cell lines
<input checked="" type="checkbox"/>	<input type="checkbox"/> Palaeontology and archaeology
<input checked="" type="checkbox"/>	<input type="checkbox"/> Animals and other organisms
<input checked="" type="checkbox"/>	<input type="checkbox"/> Clinical data
<input checked="" type="checkbox"/>	<input type="checkbox"/> Dual use research of concern
<input checked="" type="checkbox"/>	<input type="checkbox"/> Plants

Methods

n/a	Involvement in the study
<input checked="" type="checkbox"/>	<input type="checkbox"/> ChIP-seq
<input checked="" type="checkbox"/>	<input type="checkbox"/> Flow cytometry
<input checked="" type="checkbox"/>	<input type="checkbox"/> MRI-based neuroimaging

Plants

Seed stocks	not applicable
Novel plant genotypes	not applicable
Authentication	not applicable